17 October 2016

Johan Nilsson 10/16/2016 4:09 PM
Deleted: 13 October 201627 September 2016

Improved retrieval of land ice topography from CryoSat-2 data and its impact for volume change estimation of the Greenland Ice Sheet

Johan Nilsson[1], Alex Gardner[1], Louise Sandberg Sørensen[2] and Rene Forsberg[2]

[1]Jet Propulsion Laboratory, California University of Technology

[2] DTU Space, National Space Institute, Technical University of Denmark

Abstract

A new methodology for retrieval of glacier and ice sheet elevations and elevation changes from CryoSat-2 data is presented. Surface elevations and elevation changes determined using this approach show significant improvements over ESA's publically available Cryosat-2 elevation product (L2 Baseline-B). The results are compared to near-coincident airborne laser altimetry from NASA's Operation IceBridge and seasonal height amplitudes from the Ice, Cloud, and Elevation Satellite (ICESat).

Johan Nilsson 10/4/2016 10:44 AM
Deleted: ,

Applying this methodology to CryoSat-2 data collected in Interferometric Synthetic Aperture mode (SIN) over the high relief regions of the Greenland ice sheet we find an improvement in the root-mean-square-error (RMSE) of 27% and 40% compared to ESA's L2 product in the derived elevation and elevation changes, respectively. In the interior part of the ice sheet, where CryoSat-2 operates in Low Resolution Mode (LRM), we find an improvement in the RMSE of 68% and 55% in the derived elevation and elevation changes, respectively. There is also an 86% improvement in the magnitude of the seasonal amplitudes when compared to amplitudes derived from ICESat data. These results indicate that the new methodology provides

improved tracking of the snow/ice surface with lower sensitivity to changes in near-surface dielectric properties.

To demonstrate the utility of the new processing methodology we produce elevations, elevation changes and total volume changes from Cryosat-2 data for the Greenland Ice Sheet during the period Jan-2011 to Jan-2015. We find that the Greenland Ice Sheet decreased in volume at rate of 289 ± 20 $km^3 a^{-1}$, with high inter-annual variability and spatial heterogeneity in rates of loss. This rate is 65 $km^3 a^{-1}$ more negative than rates determined from ESA's L2 product, highlighting the importance of Cryosat-2 processing methodologies.

1 - Introduction

The European Space Agency (ESA) launched CryoSat-2 in April 2010 tasked with monitoring the changes of the Earth's land and sea ice. CryoSat-2 carries a new type of Doppler/delay radar altimeter (Raney, 1998) referred to as SIRAL (SAR Interferometric Radar Altimeter). SIRAL operates in two different modes over land ice. Over the interior part of the ice sheets it operates as a conventional pulse limited radar system, referred to as the "Low Resolution Mode" (LRM). In more complex high-sloping terrain the system uses a novel second antenna to operate in "Interferometric Synthetic Aperture Radar" (SIN) mode. This new feature allows the satellite to monitor changes in complex terrain including ice caps, glaciers and the high relief marginal areas of the ice sheets. Such areas are sensitive to changes in climate and contribute greatly to current rates of sea level rise (e.g., Gardner et al. (2013) and Shepherd et al. (2012)).

Johan Nilsson 10/9/2016 8:12 PM
Deleted: ese

Johan Nilsson 10/9/2016 8:13 PM
Deleted: s

Ku-band radar altimeters are insensitive to cloud cover providing superior coverage to laser altimeters (e.g., ICESat) but experience significant amounts of volume scattering, which is controlled by the time-evolving dielectric properties of the near-surface snow, firn, and ice (Lacroix et al., 2008; Remy et al., 2012). These effects can have large implications for the determination of mass change over a wide range of both spatial and temporal scales. Changing snow conditions can introduce time-varying biases in the data that, in combination with the radar

signals interaction with the surface, introduce large elevation biases (0.5 - 1 m) (Nilsson et al., 2015a). This, combined with other factors such as processing methodology and surface topography, makes it difficult to measure small changes for much of the word's ice covered regions (Arthern et al., 2001; Gray et al., 2015; Nilsson et al., 2015b).

The mitigation of these effects in the processing of radar altimetry data is required for improved accuracy of derived temporal and spatial changes in surface elevation of glaciers and ice sheets. Several studies have proposed different approaches to assess these effects and improve the retrieval process of surface elevation and elevation changes from radar altimetry data. These include different approaches to waveform retracking (Davis, 1993, 1997; Gray et al., 2015; Helm et al., 2014) and empirical corrections to the estimated surface elevation changes (Davis and Ferguson, 2004; Flament and Rémy, 2012; Sørensen et al., 2015; Wingham et al., 2006b; Zwally et al., 2005, 2011). Relatively little work has been done to assess methods for improving elevation and elevation changes derived from ESA's CryoSat-2 data (Abulaitijiang et al., 2015; Gray et al., 2013, 2015; Helm et al., 2014).

Here we conduct a thorough analysis of CryoSat-2 SIN and LRM waveform retracking, filtering and processing methodologies to design an optimal processing methodology for CryoSat-2 elevation retrieval over both smooth and complex ice-covered terrain. We then analyze two different approaches to determining surface elevation and volume changes from the scattered CryoSat-2 elevation retrievals. The overarching goal of this work is to develop robust and accurate elevation retrieval algorithms that are less sensitive to changes in surface and sub-surface scattering properties.

Johan Nilsson 10/9/2016 8:13 PM
Deleted: geolocation

Johan Nilsson 10/9/2016 8:14 PM
Deleted: several

The new processing scheme is applied to estimate elevation and volume changes of the Greenland Ice Sheet for the period January 2011 to January 2015, using two independent methods to characterize the robustness of the results due to methodology. The results are compared to change estimates obtained from the ESA L2 Baseline-B surface elevation product (Bouzniac et al., 2014), high accuracy airborne data from NASA IceBridge airborne topographic

mapper and seasonal height amplitudes estimated from Ice, Cloud, and Elevation Satellite (ICESat) data.

2 - Surface elevations from CryoSat-2

2.1 - Low Resolution Mode (LRM)

The LRM mode is used over the interior parts of the ice sheet, which mostly consist of low sloping terrain. Here, SIRAL operates as a conventional pulse limited radar system with a transmission frequency of 13.6 GHz (Ku-band) and has Pulse-Limited Footprint (PLF) radius of approximately 1.5 km and a beam-limited footprint (BLF) radius of approximately 7.5 km over flat terrain (Bouzinac, 2014). The gentle terrain allows for accurate mapping of the surface elevation of the ice sheet down to decimeter-level (Brenner et al., 2007). Within the LRM waveform we define the location of the surface from the leading edge of the waveform, based on a fraction of the maximum amplitude of the received power. This approach is commonly referred to as a threshold retracker. Following Davis et al. (1997) we use 20% threshold to define the location of the surface. Davis et al. (1997) argued that a 20% threshold represents the best compromise between waveforms that are entirely dominated by either volume or surface scattering, making it suitable for obtaining estimates of surface elevation for most parts of the Greenland Ice Sheet.

The CryoSat-2 LRM radar waveforms suffer from measurement noise, in the form of speckle noise. Furthermore, over the steeper parts of the LRM-area the range gate tracking-loop can loose track of the surface, producing non-usable waveforms. To remove bad or loss of track waveforms the radar waveform (20 Hz) is first filtered using a zero-phase low pass filter to reduce speckle noise on a line-by-line basis. The signal-to-noise-ratio (SNR) of the waveform is then estimated and if the SNR < 0.5 dB the waveform is rejected. The SNR threshold was

empirically chosen to obtain a good trade-off between the quality of the measurements and sampling.

Before the waveform can be retracked the first surface return (first major peak) is identified within the range gate window. A copy of the waveform is heavily smoothed to remove small-scale surface roughness signals, keeping the overall surface signal intact. The range gate index of the first peak from the copy is then used to extract the leading edge of the original low pass filtered waveform. Only leading edges with a peak index above 20 are used in the retracking, as peaks before or after that can indicate troublesome surface ranging. The extracted leading edge is then oversampled by a factor of 100 (c.f. (Gray et al., 2013; Helm et al., 2014), and the range R between the surface and satellite is determined based on the 20% threshold computed according to Davis et al. (1997). The range is then corrected for several atmospheric and geophysical effects relevant to land ice studies according to Bouzinac (2014). The surface elevation H of the topography, relative to the WGS84 ellipsoid, is estimated as $H = A - R$, where A is the altitude of the satellite.

The measured surface return over a sloping surface does not originate from the satellites nadir location, but from the “Point Of Closest Approach” (POCA) to the spacecraft (Brenner et al., 1983). These off-nadir returns can introduce a large range bias to the surface, depending on the magnitude of surface slope, ranging from 0-120 m (Brenner et al., 1983) as the measured surface height is mapped to an erroneous position (i.e. the nadir position). To mitigate the effect of this error we correct the measured range and location to the POCA point using an a-prior DEM, following the approach of Bamber (1994). In contrast to previous studies we account also for the local surface curvature, as Remy et al. (1989) showed that accounting for surface curvature in addition to surface slope significantly improve results. The surface slope, aspect and curvature are estimated from an a priori DEM. The GIMP elevation model (Howat et al., 2014) was used to derive surface parameters for the slope-induced error correction in the LRM mode. The DEM was resampled to 2 km resolution, using bilinear

interpolation, prior to parameter estimation, which provided the lowest root-mean-square-error and further corresponds to the pulse-limited footprint of the LRM mode.

Johan Nilsson 10/9/2016 8:15 PM
Deleted: corresponding

2.2 - Interferometric Synthetic Aperture Radar Mode (SIN)

The SIN mode is used over the marginal areas of the ice sheets and other smaller glaciated areas. In these areas the SIRAL altimeter operates as a Doppler/Delay radar system (Raney, 1998). The Doppler/Delay radar allows for higher along-track resolution compared to conventional altimetry, resulting in 350 m resolution in along track and 1500 m across track. In ordinary SAR operation only the amplitude of the radar echo is measured and the phase content is discarded or ignored. With the inclusion of a second antenna on CryoSat-2, interferometric SAR can also be performed. The difference in path length between the POCA and the individual antennas introduce a phase shift between the two retrieved signals that can be related to the angle of arrival (look angle). The look angle can in turn be used to resolve the across track (across antenna) location of the echo.

Johan Nilsson 10/9/2016 8:18 PM
Deleted: D

Johan Nilsson 10/9/2016 8:18 PM
Deleted: the

Multi-look processing is applied to ESA's L1B waveform product (Bouzinac, 2014) to reduce the noise in the SIN waveform but it is still affected by speckle-noise, as is the case for the LRM waveforms. To mitigate this effect, and to help identify the leading edge of the first return, we apply speckle reduction filtering and leading edge extraction of the SIN waveforms in the same way as for the LRM processing with minor changes due to differences in range gate resolution. In this case, compared to the LRM retracking algorithm, only leading edges with a peak index in the range of 100-350 are used for retracking the radar waveform (P_w).

Johan Nilsson 10/9/2016 8:18 PM
Deleted: 20

The estimated coherence *C* of the multi-looked waveforms is then filtered in two stages; (i) all coherence measures larger than one is set to zeros (coherence values larger than one exists in the L1B product due to unknown reasons). (ii) The coherence array, as a function of range, is filtered using a 2D 5x5 Wiener filter to remove high frequency noise. The filtering of the

Johan Nilsson 10/4/2016 10:46 AM
Deleted: larger than one

Johan Nilsson 10/4/2016 10:47 AM
Deleted: reason unknown

waveform and the coherence is applied to remove noise in the recreation of the interferogram, discussed below.

The measured differential phase ϕ of the return signal is affected by phase ambiguities; a sudden shift of 2π in the measured phase. To reduce phase noise and aid the phase, an unwrapping of the radar interferogram I is performed according to Gray et al. (2013):

$$I = P_w \cdot C \cdot e^{-i\phi} \quad (1)$$

The interferogram is then filtered using a wavelet-based de-noising technique, where the real and imaginary parts of the interferogram are filtered separately. The unwrapping of the interferogram allows for indirect filtering of the phase, without being affected by the phase-ambiguities. Phase filtering is an important consideration as it has a direct affect on accuracy of the position of the ground echo. We selected a bi-orthogonal as the mother wavelet to produce the wavelet coefficients decomposed into three levels. Soft thresholding was applied to detail coefficients, using a heuristic threshold rule to remove noise at every level. This was done on a line-by-line basis. The final filtered differential phase was then recovered by:

$$\phi_f = Re\{I_f\} + Im\{I_f\} \quad (2)$$

To resolve the phase ambiguities the filtered phase measurements require unwrapping. The phase unwrapping is done on a line-by-line basis in two directions starting from the center of gravity of the waveform (Wingham et al., 1986).

The return power distribution of a Doppler/Delay radar system shows an important distinction from those from conventional pulse-limited radar systems. Here, the point corresponding to the mean surface is not located at the half-power point on the leading edge, but rather closer to the maximum (Wingham et al., 2006a). Therefore a new retracker has been developed, closely related to the one used in Gray et al. (2013), to allow for adaptive retracking of the upper parts of the leading edge of the SAR waveform. The algorithm follows the main concept of the threshold retracker, developed by Davis (1997), but instead of a pre-defined

Johan Nilsson 10/17/2016 2:19 PM
Deleted: . This is further discussed later

Johan Nilsson 10/17/2016 2:21 PM
Deleted: P

Johan Nilsson 10/4/2016 10:48 AM
Deleted: ,

threshold it tracks the maximum gradient of the leading edge of the oversampled waveform. We refer to this approach as that “Leading-edge Maximum Gradient retracker” (LMG).

The surface returns are geolocated using the across track look-angle θ estimated from the differential phase at the retracking point according to (Wingham et al., 2006a). This, in combination with the viewing geometry, is used to define the location of the surface return on the ground using basic across track interferometric principles. We correct θ for the interferometer surface slope error by applying the look-angle scaling factor estimated in (Galin et al., 2013).

Johan Nilsson 10/4/2016 10:48 AM
Deleted: retrackig

The along-track differential phase estimate, interpolated to the retracking point, is affected by phase ambiguities not corrected for during the phase unwrapping procedure. To reduce residual phase ambiguities an a priori DEM (GIMP) is used to extract the DEM surface, resampled to 500 m resolution (corresponding roughly to the along-track sampling), elevations at the nadir and echolocation using bilinear interpolation. Over a sloping surface the surface return should always come from a position upslope from the nadir point. Therefore the following relation must hold where ($H_{echo} > H_{nadir}$) or for a more practical application ($H_{echo} - H_{nadir}) > \varepsilon$, where ε is the uncertainty of the DEM used. If this relation is violated 2π is added or subtracted to the individual along-track phase estimate, depending on the sign.

A final step is applied to correct for any lingering phase ambiguities not corrected by the a priori DEM. This step uses the assumption that the along-track phase should follow a consistent pattern over most part of the satellite ground track. Hence, any large discrepancies from the overall pattern of the along-track phase would indicate an ambiguity. The ambiguity is detected by computing the residuals of the along-track phase by removing a smoothed version of the differential phase. If any of the residuals have a magnitude larger than π it is considered ambiguous and thus corrected by adding or subtracting 2π.

3 - Surface elevation changes from CryoSat-2

3.1 – Surface fit method

The surface-fitting method is based on fitting a linear model to the elevations as a function of time and space inside a search radius of 1 km (e.g., Howat et al., 2008; Moholdt et al., 2010; Sørensen et al., 2011; Wouters et al., 2015). The linear model consists of a time-invariant (static) bi-quadratic surface model to account for variable topography inside the search radius and time-variant part used to extract the temporal change in elevation. The model consists of a total of 7-parameter whereof six of the parameters (a-coefficients) describe the bi-quadratic surface modeling function, *dh/dt* the linear elevation change rate, *t* time in decimal years, t_0 the mean time inside the footprint and ε the residuals from the linear regression.

$$h(x,y,t) = a_0 + a_1 x + a_2 y + a_3 xy + a_4 x^2 + a_5 y^2 + \frac{\partial h}{\partial t}(t - t_0) + \varepsilon \quad (3)$$

The algorithm estimates the elevation change at every echolocation (or grid-node if desired) in the data set. In each solution the signal amplitude and phase are also estimated by fitting a seasonal signal model to the surface-fit elevation residuals, according to:

$$\Delta h(t) = s_0 \cos(wt) + s_1 \sin(wt) + \varepsilon \quad (4)$$

where Δh is the elevation residuals estimated from the plan-fit model, $s_{0,1}$ are the model coefficients and t the time. The amplitude *A* is then defined as $A = \sqrt{s_0^2 + s_1^2}$ and the phase *P* as $P = \tan^{-1}\left(\frac{s_1}{s_0}\right)$.

To remove outliers an iterative 3σ-filter is used in the full model solution, i.e. the topography, trend and seasonal signal are removed, using a maximum of 5-iterations. For each iteration residuals (full-model) with an absolute value larger than 10 m are removed, as seasonal changes larger than 10 m are not expected (Moholdt et al., 2010; Qi and Braun, 2013). The data inside the 1 km cap is weighted according to their distance from the estimation point according to:

$$W = \frac{1}{\left(1+\left[\frac{d}{\rho}\right]^2\right)} \quad (5)$$

where W is the estimated weight, d the distance and ρ the correlation or resolution parameter set to 500 m. The weighting allows the solution to better reflect local signal dynamics at the prediction point.

Local elevation time-series are further computed from the elevation residuals and elevation trend from each solution, according to:

$$h(x, y, t) = (t - t_0) \cdot \frac{\partial h}{\partial t} + \varepsilon \quad (6)$$

where t is the time epochs inside the search cap, t_0 is the mean time of t, dh/dt is the estimated elevation change rate and ε is the elevation residual at each time epoch.

The elevation changes estimated from the surface-fitting method are then culled to remove outliers before spatial gridding. Elevation changes with a regression error larger than 15 m a^{-1} are removed. The resulting surface elevations are binned at 5-km resolution for outlier editing purposes. For each cell the local spatial trend is modeled as a bilinear surface, and removed. The residuals are then edited using an iterative 3σ filter until the RMS converges to 2%.

3.2 – Crossover method

The crossover method is used to derive the surface elevations at the intersection point between an ascending and descending satellite ground track separated in time (Brenner et al., 2007; Khvorostovsky, 2012; Zwally et al., 1989). The surface elevations and times are then estimated at the crossover location for each track by linear interpolation of the two closest data points for each ascending and descending track. The crossover height difference is then estimated by taking the height difference between the two tracks according to:

$$\Delta h = h_2 - h_1 + \varepsilon \quad (7)$$

were h_1 and h_2 are the surface heights at the crossover location at time epoch t_1 and t_2, respectively, and E is the random measurement error, including orbital, range and retracking errors.

This approach produces crossover height differences with scattered time-epochs ranging from 0-4 years. CryoSat-2 has a 369-day repeat orbit configuration with a 30-day sub-cycle meaning that each crossover location will be revisited every 369 days and surrounding area every 30 days. This produces annual and sub-annual crossover difference around each crossover location. This fact is used to produce elevation change rates by incorporating all multi-temporal crossover difference within a neighborhood of 2.5-km around each crossover location. The elevation change is then estimated using the same procedure described for the surface-fit method, except that a bilinear model is used to remove any spatial trends in the topography of the crossover elevations according to:

$$dh(x, y, t) = a_1 x + a_2 y + \frac{\partial h}{\partial t}(t - t_0) \quad (8)$$

where *dh* is the crossover height difference, *t* the time, t_0 is the mean reference time inside the footprint, a_1 and a_2 the across and along-track slope and *dh/dt* the elevation change rate. This produces elevation changes comparable in time and in spatial coverage with the surface-fit method. The same outlier editing schemes is applied to the crossover elevation change rates as for the surface-fit method.

Johan Nilsson 10/9/2016 8:24 PM
Deleted: (

Johan Nilsson 10/9/2016 8:24 PM
Deleted: -t_0)

Johan Nilsson 10/9/2016 8:24 PM
Deleted:

Johan Nilsson 10/9/2016 8:24 PM
Deleted: difference

3.3 - Gridding of sparse elevation and elevation change data

The gridding is done in a polar-stereographic projection with a latitude of origin at 70°N, central longitude of 45°W and origin at the North Pole. The projection is referenced against the WGS-84 ellipsoid and the grid-resolution. The observations derived from the surface-fit and crossover method are gridded at a resolution of 1x1-km, due to the high spatial sampling.

The method of Least Squares Collocation (LSC), described in Herzfeld (1992) is used to grid the observations onto a regular grid. LSC is similar to Kriging and allows for optimal interpolation and merging of data with different accuracies, using their inherent covariance structure. The LSC-algorithm uses the 25 closest data points in 8-quadrants surrounding the prediction point to reduce spatial biasing. The prediction equation consists of two terms where the first term is the actual prediction term and the second term accounts for the non-stationary part of the data, as described by:

$$\hat{s} = C_{sz}(C_{zz} + N)^{-1}z + \left(1 - \sum (C_{sz}(C_{zz} + N)^{-1})\right) m(z) \quad (9)$$

were $C_{\hat{s}z}$ is the cross-covariance, C_{zz} is the auto-covariance, N the diagonal noise-matrix consisting of the a priori RMS-error and $m(z)$ is the median value of the observations inside the search neighborhood.

The covariance of the data inside the local neighborhood is modeled as a function of distance away from the prediction point using a third-order Gauss-Markov model described below.

$$C(r) = C_0 \left(1 + \frac{r}{\alpha} - \frac{r^2}{2\alpha^2}\right) e^{\left(-\frac{r}{\alpha}\right)} \quad (10)$$

where r is the separation distance, C_0 the local data variance and α is a scaling factor estimated from the correlation length.

LSC interpolation provides a RMS-error for each prediction point estimated from the modeled covariance of the data according to:

$$C_{\hat{s}} = C_0 - C_{sz}(C_{zz} + N)^{-1}C_{sz}^T \quad (11)$$

where the RMSE of the prediction equals to $\sigma_{\hat{s}} = (C_{\hat{s}})^{1/2}$ and where $C_{sz}{}^T$ is the transposed cross-covariance matrix.

The elevation changes estimated from the surface-fit and crossover methods are interpolated to a regular grid using their a priori error estimated from the LSC scheme. To avoid unrealistically small errors, common in the regression errors estimated over flat terrain, a

minimum error threshold is applied. Error values smaller than a specific threshold are set to the threshold value. The threshold value is representative of the overall precision of the elevation changes over flat terrain and is set to 0.2 m a^{-1}. The data are then gridded using a 75 km correlation length determined from the comparison of CryoSat-2 elevation to airborne measurements (Section 5).

The LSC algorithm is also used to generate a DEM based on the surface elevations generated from the surface-fitting algorithm. The surface elevations generated from the surface-fit were used as input to the gridding-algorithm. The use of surface elevations from the surface-fit provides several advantages compared to the raw observations as they: provide an almost equal number of observations as the raw data, have been screened for gross outliers, have been low-pass filtered using the 1-km search radius, and are all reference to roughly the same time epoch. Further the RMSE error generated from the surface-fit estimated surface height can be used as an a priori error for the LSC gridding procedure.

The DEM is generated using the same approach as for the surface elevation changes, as described previously in the section. Before the gridding procedure is applied elevations $H < 0$ and $H > 3350$ m are removed from the data set. Further, elevations with a standard error larger than 30 m are also removed. The elevations are binned spatially into a resolution of 1000 m and inside each cell the local surface trend is removed by fitting of a planar surface, and an iterative 3σ filter is applied to the residuals to remove outliers.

4 - Surface elevations and elevation changes from ICESat

To assess basin-scale patterns of elevation change we compare elevation changes from CryoSat-2 data to elevation changes derived from Ice, Cloud, and Elevation Satellite (ICESat) data. Here we use release 33 (GLA06) data collected over the 2003-2009 period. The ICESat surface heights were used to generate surface elevation changes and seasonal parameters

according to method M3 in Sørensen et al. (2011). The derived elevation changes were corrected for the G-C offset (Borsa et al., 2014). Valid elevation retrievals were selected according to Nilsson et al. (2015b). The ICESat elevation, seasonal amplitude and phase, are then used for comparison with CryoSat-2 and to build continuous time series using the surface fit method described in Section 3.1. For the purpose of this study no correction for the inter-campaign bias was applied, as this is still an active area of investigation.

5 -Validation

Elevation and elevation change results were generated for the entire Greenland Ice Sheet using CryoSat-2 data collected between Jan-2011 and Jan-2015 using the methodology presented in (Sections 2-3) (JPL product) and by applying the methods of (Section 3) to ESA's CryoSat-2 L2 elevation products (ESA product). Surface elevations and elevation changes were validated against airborne data sets obtained from NASA's Operation Ice-Bridge Airborne Topographic Mapper (ATM), obtained from the "National Snow & Ice Data Center" (NSIDC) in the form of the ILATM2 product. The generated elevation product has a resolution of 80 m, with a 40 m spacing along-track. This mission produces both elevation and elevation changes with reported vertical accuracy of ~10 cm and temporal accuracy in the cm-level (Krabill et al., 2002).

The derived surface elevations from CryoSat-2 are differenced against ATM surface elevations within 50 m of each ATM locations. One month of CryoSat-2 data consistent in time with the ATM elevations are used for the validation to avoid biases due to temporal sampling and to obtain sufficient sample size. A total of four years of campaign data are used for the validation of the surface elevations (2011-2014). The residuals are edited using an iterative 3σ filter to remove outliers. The accuracy and precision is estimated as the mean and standard deviation of the differences, respectively. The residual distribution is further binned according to surface slope estimated from the GIMP DEM (Howat et al., 2014) resampled to 500 m. The sensitivity to surface slope (slope error) can be identified in the standard deviation of the binned

residuals and can be used to judge the quality of the produced surface elevation and elevation changes, while the binned-average for the elevations can be used to determine radar-signal penetration depth.

Surface elevation change rates estimated from three different time-periods (2012-2014, 2011-2013 and 2011-2014) of overlapping ATM observations (Krabill, 2014) are used to validate the surface elevation changes estimated from the CryoSat-2 data. The same validation methodology applied to surface elevations is applied to surface elevation changes, with a few minor modifications. First the search radius is increased to 175 m to make it conform to the ATM elevation change resolution of 250 m, as this search radius encloses the entire ATM grid cell. Secondly the estimated mean and standard deviation are multiplied with the individual time-intervals of the validation data sets to make the errors comparable, as they differ in time span.

For the surface-fit and crossover methods, near-coincident elevation change rates were compared with ATM rates (e.g., April-2011 to April-2014). This provided three validation data sets for the surface-fit method, due to its high spatial coverage. However, only the 2011-2014-validation data set could be used for the crossover method, due to the lower spatial sampling of the crossovers.

The overall accuracy and precision for both the surface elevation and elevations changes are then estimated by taking the weighted mean, using the number of observations as weights, for each data set giving an average error for each measurement mode, as seen in Table-2. The weighted average errors for each mode and method have been summarized in Table-1 and Table-2 for both the ESA's and our solutions, where the values for the individual campaigns can be found in the Supplementary material.

The estimated surface elevation changes from the two independent methods were validated separately using near-coincident ATM data. The statistics of the elevation change validation have been summarized in Table-2 for each method independently for the two modes of instrument operation. We find the lowest RMSE errors for the surface-fit method, followed by

Johan Nilsson 10/9/2016 8:27 PM
Deleted: . In general we find the same magnitude of improvement observed in the surface elevation validation analysis

388 the crossover method. This differs from the findings of Moholdt et al. (2010) who found lower
389 intrinsic errors for the crossover method, compared to the surface-fit method when applied to
390 ICESat data. The larger search radius used for our application of the crossover method most
391 likely explains the difference in findings between the two studies. Further, we find that the
392 surface-fit method provides the largest reduction in RMSE for the JPL product, corresponding to
393 40% and 55% for the SIN and LRM-mode, respectively.

394 The correlation length used to derive the number of un-correlated grid-cells, which is
395 used to estimate the standard error, was determined from a semi-variogram analysis of the
396 elevation change residuals from CryoSat-2 minus ATM using the data from the surface-fit
397 method. The comparison was done for each mode separately for all the individual campaigns
398 and multiplied with the their individual time span. The semi-variogram was then computed from
399 all the time-invariant residuals, to maximize the spatial coverage, for each mode. Analysis of the
400 semi-variogram showed approximate correlation lengths of 100 and 75 km for the SIN and
401 LRM-mode respectively. These correlation lengths are inside the range of the ones found by
402 Sørensen et al. (2011) for their analysis of ICESat data, which was found to be between 50-150
403 km.

404 The main goal of this study is not to derive or compare different types of DEM's.
405 However, to gain insight into the overall quality of our CryoSat-2 derived DEM (referred to as
406 JPL) we compare it to three other DEM's derived from other data sets. Firstly, we compare it to
407 a DEM derived from ESA CryoSat-2 L2 data (referred to as ESA) gridded in the same manner
408 as our DEM (Section 3.3). Secondly we compare it to a DEM from Helm et al. (2014), also
409 based on CryoSat-2 data from 2011-2014 (referred to as AWI). Thirdly, we compare to a DEM
410 from Howat et al. (2014) (which was used to derive topographical parameters and corrections
411 for the JPL CryoSat-2 data), based on photogrammetry and altimetry data from the mid 1990's
412 to 2010 (depending on data source), co-registered to ICESat elevation data from 2003-2009
413 (referred to as GIMP).

Johan Nilsson 10/9/2016 8:29 PM
Deleted: Although the main goal of this study is not to derive or compare different types of DEM's they do play a critical part in removing the long-wavelength topography in order to derive the monthly time-series of volume change from the DEM-method

Johan Nilsson 10/9/2016 8:28 PM
Deleted: .

Johan Nilsson 10/9/2016 8:28 PM
Deleted: T

Johan Nilsson 10/9/2016 8:30 PM
Deleted: s

Johan Nilsson 10/9/2016 8:32 PM
Deleted: .

Johan Nilsson 10/4/2016 11:11 AM
Deleted:

Johan Nilsson 10/4/2016 11:09 AM
Deleted: from

Johan Nilsson 10/4/2016 11:09 AM
Deleted: 1999-2002

These data sets were then compared to IceBridge ATM elevations, spanning the four different campaigns previously used for validation of the CryoSat-2 elevations. The DEM elevation was estimated at each ATM location, using bilinear interpolation, and the elevation difference computed as (DEM-ATM). No attempt was made to account for differences in DEM and ATM epochs. The estimation of the errors of the DEM was determined in the same way as for the individual CryoSat-2 surface heights. The results of the comparison have been summarized in Table-3, as the weighted average of the different campaigns. The values from each individual campaign can be found in the supplementary material.

Analyzing the overall RMSE we find that the AWI produces the lowest RMSE, followed by JPL, ESA and GIMP, due to AWI's lower standard deviation. However, the best accuracy is obtained by the JPL DEM, which shows the lowest elevation bias of all DEM's. The ESA derived DEM shows a slightly better standard deviation than the JPL DEM, which can be explained by higher data density in the marginal areas for the ESA data. The difference in density is due to the SNR rejection criterion applied in our elevation processing. The lower standard deviation in the AWI product is mostly likely due the use of lower resolution topography in many of the high relief areas in the 1 km elevation model, producing a smoother estimate of the surface. The GIMP data set showed higher degrees of impulse noise than the other products, explaining the higher observed standard deviation. This impulse noise is attributed to that local elevation change rate, which was not accounted for in the creation of the DEM (Howat et al., 2014). Overall we find that the JPL DEM provides a suitable compromise between resolving of local detail and the minimization of bias. Further, modification to the SNR filtering criteria will likely lead to additional improvements in the DEM.

Johan Nilsson 10/9/2016 8:33 PM
Deleted: is smoothing can explain the lower standard deviations seen for the AWI product

To determine the effect of retracking on the accuracy and precision of the measured surface heights from CryoSat-2 several tests was performed over different parts of Greenland for both modes. Following the approach of Davis (1997) the accuracy (mean) and precision (standard deviation) was computed as a function of leading edge threshold (in percent). This

computation was performed using a standard leading-edge threshold retracker, referred from now on as LTH, for both the LRM and SIN mode independently. The validation was performed in the same manner as described in Section 5, where ATM elevations from 2013 was used as the surface reference.

For the LRM mode data from April 2013 from the northern parts of Greenland, spanning the region 75-81°N and 54-44°W around the North Greenland Eemian Ice Drilling camp (NEEM), was used to calculate height residuals for the different thresholds. This produced approximately 1000 comparison locations, which was used to calculate statistics. The same procedure was performed over Jakobshavn Isbræ, using the same time span, to calculate statistics for the SIN-mode providing roughly 2500 comparison locations.

The results of this analysis, summarized in Figure-2, show that for the LRM-mode the precision (as a function of threshold) follows the same behavior as observed by Davis (1997), with a decrease of precision following increasing retracking threshold. However, the most notable finding was the observed inverse relationship in precision for the SIN-mode compared to LRM. For LTH-algorithm, in the SIN-mode, we observe a clear increase in precision as the retracking threshold increases, seen in Figure-2, stabilizing around 30-40%.

Analyzing the accuracy derived from the different thresholds a clear difference in apparent penetration depth of the radar signal can be observed for the two modes. For the SIN-mode, below 40%, a positive bias is observed indicating that retracker produces elevations larger than the corresponding airborne measured heights. For thresholds larger than 40% surface penetration of the signal is observed which are in general closer to the surface compared to the LRM-mode. We attribute this to differences in the near-surface density structure covered by the two modes.

In general we conclude that for the LRM-mode applying low retracking thresholds (0-30%) reduces the magnitude of the apparent surface penetration bias and provides higher precision compared to higher thresholds. Therefore, a threshold of ~20% of the leading edge is

Johan Nilsson 10/4/2016 11:29 AM
Deleted: that

Johan Nilsson 10/4/2016 11:29 AM
Deleted: that

suggested for retracking surface elevations for the LRM-mode, which was also previously suggested by Davis (1997) and Helm et al. (2014). However, for the SIN mode a threshold below 40% is not recommended, as this produces a clear positive elevation bias and poor precision, as seen in Figure-2. Analyzing the difference between the LTH and the adaptive LMG algorithm, used in the SIN-mode, we find that the LMG algorithm produces superior results in precision compared to the standard LTH-algorithm. Comparing the adaptive solution from LMG to the optimum threshold found by the LTH-algorithm, we find a comparable magnitude of the elevation bias and a 32% improvement in precision, with an overall 27% reduction in RMSE, using the LMG-retracker. From this comparison between the two-retracker algorithms we recommend the use of the adaptive threshold approach (LMG), as it produces an elevation repeatability that exceeds that of the standard threshold retracker (LTH) and provides a low penetration bias.

A case study was also performed to determine the different processing steps effects on the quality of the retrieved elevations. For this purpose the Barnes ice cap, on Baffin Island in the Canadian Arctic, was chosen due to its small size, excellent validation coverage and due to that it consist mostly of super-imposed ice (reducing radar signal penetration). The ice cap saw a major IceBridge ATM campaign in 2011 providing a large number of flight tracks (spanning in both North-South and East-West directions) suitable for validating CryoSat-2 data. The result of this case study, which is detailed in supplementary material (i.e. Table-S1) shows that the filtering of the differential phase has the highest impact on the overall accuracy of the observation, reducing the RMSE by 12%, followed by the ambiguity correction. This shows the importance of these steps, as they can have important implications for the overall quality of the retrieved elevations. This is especially true in high relief areas where small changes in the look angle, or an introduced phase ambiguity, can produce large elevation errors ranging from 0-100 m in elevation (Brenner et al., 1983).

Johan Nilsson 10/9/2016 8:42 PM
Deleted: Studying the results from this

Johan Nilsson 10/4/2016 11:30 AM
Deleted: affect

Johan Nilsson 10/9/2016 8:43 PM
Deleted: observations

Johan Nilsson 10/4/2016 11:30 AM
Deleted: with

6 - Error analysis

To compute volume change errors for the two methods we divide the error budget into two main components (1) the observational standard error (ε_{obs}) and the interpolation standard error (ε_{int}). The observational error budget is estimated using the root-mean-square error (RMSE) of the difference between CryoSat-2 and airborne elevation change differences, as described in Section 5. The RMSE is estimated separately from the two different modes, with the total volume change error (ε_{vol}) being computed as the RSS of the standard elevation change error of the two modes and their corresponding area, according to:

$$\varepsilon_{vol} = \sqrt{(\varepsilon_{lrm}\, A_{lrm})^2 + (\varepsilon_{sin}\, A_{sin})^2} \quad (12)$$

were A_{lrm} and A_{sin} are the areas covered by each mode. The ε_{lrm} and ε_{sin} are the standard elevation change errors of the LRM and SIN computed from the airborne validation data sets.

The observational elevation change error is estimated from the residual elevation change differences in Table-2 for the two methods. The RMSE from the LRM/SIN errors are computed using Gaussian error propagation producing an observational elevation change error (σ_{obs}). For the surface-fit and the crossover method the interpolation error is estimated as the RMS of the LSC uncertainty grid, defined as (σ_{int}). The final elevation change error is then estimated by combing the two error sources using RSS according to:

$$\varepsilon_{mode} = \varepsilon_{dh/dt} = \sqrt{(\varepsilon_{obs})^2 + (\varepsilon_{int})^2} = \sqrt{\left(\frac{\sigma_{obs}}{\sqrt{N}}\right)^2 + \left(\frac{\sigma_{int}}{\sqrt{N}}\right)^2} \quad (13)$$

Here, N is the number of uncorrelated grid-cells estimated from empirical semi-variogram analysis of the CryoSat-2 and airborne elevation change differences, and estimated according to:

$$N = \frac{A_{mode}}{\rho_{mode}^2} \quad (14)$$

were A_{mode} is the total area of the Greenland Ice sheet (~1.7x10^6 km^2) and the correlation length ρ_{mode} of 75 and 100 km for the LRM and SIN mode respectively.

Johan Nilsson 10/5/2016 3:18 PM
Deleted: three

Johan Nilsson 10/5/2016 3:28 PM
Deleted: error

Johan Nilsson 10/9/2016 8:44 PM
Deleted: corresponding

Johan Nilsson 10/9/2016 8:47 PM
Deleted: ε

Johan Nilsson 10/9/2016 8:45 PM
Deleted: c

7 – Results

7.1 – Surface elevations compared to ATM

The measured surface elevations from the two CryoSat-2 products (JPL vs. ESA) showed large differences in both accuracy and precision of the elevation measurements, as seen in Table-1. The average accuracy and precision for the LRM-mode from the two products showed values of 0.00 ± 0.43 m and -1.06 ± 0.89 m for the JPL and ESA products respectively. This corresponds to an average reduction in RMSE of 68% for the JPL product compared to the ESA LRM L2 data. Further, our product shows a lower residual slope error (seen in Figure-1c below ~0.5°) indicating a lower sensitivity to the degradation of performance as the surface slope increases.

Surface elevations generated from the SIN-mode showed the same type of improvement as for the LRM-mode. Here, an average accuracy and precision was found to be -0.52 ± 0.58 m and -0.90 ± 1.05 m for the JPL and ESA SIN elevation products respectively. This further corresponds to a reduction in the average RMSE of 27% for the JPL product compared to the ESA product. For the SIN-mode the JPL processing produces a slightly lower residual slope error, compared to the ESA processor (seen in Figure-1c above ~0.5°)

Larger improvements can be observed if separating the RMSE into its mean and standard deviation, corresponding to the accuracy and precision of the measurements. Using these definitions the analysis found that there is a 45% and 52% increase in precision for the SIN and LRM mode respectively, compared to the ESA L2 product, and a 42% and 99% improvement in accuracy for the respective modes.

The implementation of the LMG SIN retracking algorithm was found to reduce noise in the retrieved surface elevations compared to conventional threshold retracking. Though roughly comparable in accuracy, the LMG shows overall higher precision over all comparable leading

edge thresholds. The adaptive nature of the algorithm provides improved estimates of surface elevation and a good trade-off between accuracy and precision.

Johan Nilsson 10/9/2016 8:52 PM
Deleted: and gives

The 20% threshold retracker implemented in the LRM-mode was also found to provide improved estimates of surface elevation (both in accuracy and precision) compared to the model-based ESA-L2 retracker. Further, it also showed lower sensitivity to the 2012 melt event, due to the lower threshold used on the leading edge of the waveform.

7.2 – Surface elevation changes compared to ATM

The estimated surface elevation changes generated from the surface-fit method also showed improvement in the estimated accuracy and precision, as seen in Table-2. Here, an overall improvement in RMSE of 55% and 40% in the LRM and SIN mode, respectively, was found when comparing against ESA L2 generated elevation changes from the same method. The average accuracy and precision, compared to ATM generated elevation changes, was found to be 0.11 ± 0.67 m (LRM) and 0.30 ± 0.58 m (SIN) for the JPL derived changes. This compared to 0.25 ± 1.51 m (LRM) and 0.34 ± 1.06 m (SIN) for the ESA derived changes. This corresponds to an increase in elevation change accuracy of 56% and 12% for the LRM and SIN-mode, respectively, for the JPL product compared to ESA L2 elevation changes. The estimated elevation changes also show an increase in precisions for the JPL product of 56% and 45% for the LRM and SIN-mode, respectively, compared to its ESA counterpart.

The estimated elevation changes of the Greenland Ice Sheet, excluding the peripheral glaciers, over the period January 2011 to January 2015 show significant differences between products (JPL and ESA) in both spatial patterns and the total magnitude (Figures 3 & 4). The estimated volume change rate from the surface-fit method is -289 ± 20 $km^3 a^{-1}$ for the JPL-product and -224 ± 38 $km^3 a^{-1}$ for the ESA-product with a mean difference of 65 $km^3 a^{-1}$. The surface-fit and crossover-method produced on the order of ~20 million and ~2.5 million usable elevation changes, respectively, providing high spatial sampling. Due to the constraint put into

591 the JPL processor the ESA L2 data produced slightly more surface-fit observations (~10%), as
592 more surface elevations were accepted.
593 The ESA product produces a more positive elevation change pattern, which can be
594 attributed to the 2012 melt event that introduced a large positive bias with a magnitude of ~0.5
595 m (Nilsson et al., 2015a). Larger differences in the marginal areas for the surface-fit methods
596 are also observed. The positive signal detected in the interior of the ESA surface-fit-solution can
597 also be found in the basin time series, correlating well with the timing of the summer of 2012
598 melt event, which for example can be seen in the time series in Figure 3. These results are in
599 agreement with earlier work demonstrating the sensitivity of the ESA retracker to the changes in
600 the volume/surface scattering ratio (Nilsson et al., 2015a).
601 We used ICESat and CryoSat-2 derived surface heights to generate time series over
602 three regions in Northeast area of Greenland (Zachariæ Isstrøm, Nioghalvfjerdsfjorden and
603 Storstrømmen glaciers) for comparison purposes. These areas have in recent time shown large
604 and rapid changes, which has been noted by, e.g., Khan et al. (2014). The selected areas were
605 defined using hydrological basins derived by Lewis and Smith (2009), seen in (Figure 6), and
606 were further divided into smaller areas around the termini to highlight performance for areas of
607 rapid change. The ICESat and CryoSat-2 surface heights were then used to generate annual
608 time-series from 2003-2015 using (Equation 6) in the surface fit method. The estimated 12 year
609 time series show overall comparable elevation change rates over both time periods (2003-2009
610 and 2010-2015), especially in the terminus areas, providing confidence that CryoSat-2 can
611 actually monitor changes in these areas.
612
613

Johan Nilsson 10/9/2016 8:53 PM
Deleted: These are particularly noticeable in eastern Greenland (near 73.5 degrees in latitude Figure 3) where the ESA data shows marginal areas of rapid thinning that are not visible in the JPL solution.

Johan Nilsson 10/5/2016 3:22 PM
Comment [1]: Added time periods

7.3 – Seasonal phase and amplitude compared to ICESat

The amplitude of the seasonal signal (Equation 4) estimated from the surface-fit (SF) method show large differences in both magnitude and spatial variability (Figure 5). For the surface-fit method a difference in amplitude of 54% is observed between the ESA and JPL products, corresponding to area-averaged amplitude of 0.17 m or the JPL product and of 0.37 m for ESA product. The comparison with ICESat derived amplitudes from 2003-2009 estimated in (Sasgen et al., 2012) using the same methodology as used here produced an area-averaged amplitude of 0.13 m, which is in good agreement with the JPL derived amplitude. This agreement is also spatially consistent, as seen in (Figure 5), indicating low sensitivity to seasonal changes in scattering regime of the upper snowpack. The observed difference in amplitude bias, taking ICESat as the true surface amplitude while acknowledging that no inter-campaign bias has been applied and further the differences in epochs, is 0.03 ± 0.13 m for the JPL product and 0.21 ± 0.27 m for the ESA product. The smallest differences are observed at high altitudes above 2000 m a.s.l., where the three data sets show almost constant amplitude of 0.1 m (ICE/JPL) and 0.2 m (ICE/ESA), providing a factor of two larger amplitude for the ESA product. Below 2000 m a.s.l., corresponding well to the equilibrium-line-altitude (ELA) of the Greenland Ice Sheet (Poinar et al., 2015), a rapid increase in amplitude is observed for all products. This is especially true for the ESA product, which increases its magnitude by a factor of two.

Analyzing the amplitude patterns on a regional drainage basin level (Figure 5c) we find good agreement between JPL CryoSat-2 and ICESat amplitude with ESA data producing consistently larger amplitudes. Regionally, the highest amplitudes can be observed in the SE of Greenland in basins (3,4,5) and are consistent with regional precipitation patterns that show high average precipitation in these areas (Bales et al., 2009; Ettema et al., 2009).

The seasonal phase of the peak in amplitude of the seasonal cycle is shown in (Figures 5b and 5c) and shows generally good agreement between the two data sets, providing the timing of the maximum of the accumulation signal, before the onset of melt, to the months of June/July for both JPL and ESA CryoSat-2 data sets. The ICESat derived seasonal phase shows a higher dependence on elevation where the maximum of the accumulation signal is found in late May below 2000 m and late July/August above 2000 m in elevation. The ICESat discrepancies from the CryoSat-2 data are found in specific basins. Disagreements between the retrieved phase of the peak amplitude from Cryosat-2 and ICESat data are due to differences in temporal sampling as discussed in more detail in Section 8.

7.4 – Volume change

The two volume change methods produce consistent results from JPL derived elevation changes, with a difference of around 1 $km^3 a^{-1}$. The spread between volume change methods is larger (50 $km^3 a^{-1}$) when using ESA L2 data. The larger discrepancy can be mostly related to the sensitivity of the various methods to the melt event. The surface-fit method produces the most negative number (least affected by the melt event and has the lowest estimated error) and is therefore taken as the most reliable estimate for both the JPL and ESA solution.

Comparing the estimated volume change to other studies using CryoSat-2 we find that the JPL product is less negative than that estimated by Helm et al. (2014): -375 ± 24 $km^3 a^{-1}$. This difference can be attributed to difference in processing methodology and to the different epoch of the data used by Helm et al. (2014) of January 2011 to January 2014. Using the corresponding epoch the JPL data gives a volume change estimate, based on the surface-fit method, of -353 ± 26 $km^3 a^{-1}$, well within the stated uncertainty of Helm et al. (2014).

To examine the regional behavior of volume change estimates of the Greenland Ice Sheet, gridded values from the two methods were divided into 8-drainage basins according to Zwally et al. (2012). When analyzing the elevation time-series at the basin scale clear

Johan Nilsson 10/9/2016 8:56 PM
Deleted: products

Johan Nilsson 10/9/2016 9:01 PM
Deleted: 1

Johan Nilsson 10/5/2016 3:24 PM
Formatted: Indent: First line: 0.5"

Johan Nilsson 10/5/2016 3:18 PM
Deleted: three

Johan Nilsson 10/5/2016 3:17 PM
Deleted: volume change

differences can be observed in the annual and inter-annual behaviors (Figure 4). The northern and interior basins (1, 2, 7, 8) all exhibit large differences (Table 4: 0 - 30 $km^3 a^{-1}$) in the estimated volume change rates due to changes in the scattering regime resulting from the 2012 melt event. In the majority of the southern basins (4, 5, 6, 7), located in areas with higher precipitation, both products show good agreement in both trends and seasonal amplitude estimated from the surface-fit method.

8 - Discussion

The CryoSat-2 processing methodology presented here is found to produce accurate and precise measurements of ice sheet elevation and elevation change. The main improvements have been introduced in the SIN processor with the inclusion of a novel type of land ice retracker (LMG), advanced phase filtering and the inclusion of a phase ambiguity correction scheme. This processing approach decreased the RMSE in the surface height retrieval by approximately 27% (45% and 42% improvement in precision and accuracy). This improvement further propagated into the quality of the estimated elevation changes for the SIN-mode, with the same magnitude of improvement (Table-2). The described SIN-processing also generated surface elevations and elevation changes with lower sensitivity to the local surface slope, indicating a higher degree of accuracy in the geolocation and surface range estimation.

The SIN processing methodology further includes a phase filtering and phase ambiguity correction scheme. Visual inspections of a large number of tracks have shown more coherent estimation of the surface locations in the JPL product and further the implementation of the phase-ambiguity correction greatly reduced the number of track offsets. It was also noted that a relatively course DEM (~1 km) could be used to resolve phase ambiguities. The detection and correction of phase ambiguities are relatively straightforward and rely mostly on the relative accuracy of the DEM. The implementation of the phase ambiguity correction is particularly

Johan Nilsson 10/9/2016 9:02 PM
Deleted: ew

Johan Nilsson 10/9/2016 9:02 PM
Deleted: -

Johan Nilsson 10/9/2016 9:02 PM
Deleted: our

699 important when monitoring smaller ice caps and outlet glaciers, where frequent and large track
700 offsets can bias the estimation of the underlying topography.

701 The new LRM processing methodology focused on optimal retrieval of surface
702 elevations over the interior parts of the ice sheet. Here the choice of retracking threshold has
703 proven to be the critical factor to acquire high quality surface elevations and elevation changes.
704 The choice of 20% leading edge threshold level reduced the sensitivity to changes in the
705 scattering regime for low slope, high elevation areas. The functional-based retracking algorithm
706 used in the ESA LRM processor corresponds roughly to a 50% threshold level (Wingham et al.,
707 2006a), which appears to suffer from a higher sensitivity to changes in the scattering properties
708 (volume scattering) of the near-surface firn, as the range is reference higher up (later in time) on
709 the leading edge of the waveform. This effect can be seen in Figure 2a, and that the observed
710 negative elevation bias (Table-1) for ESA-LRM (-1.0 m) fit well with the bias for the 50% LRM
711 threshold value shown in Figure 2a. This makes the algorithm more sensitive to annual and sub-
712 annual changes in snow-packs volume/surface scattering ratio, which can produce spurious
713 changes in elevation due to changes in the near surface dielectric properties. This is clearly
714 shown in patterns of ESA product derived elevation changes (Figure 3) where a large elevation
715 bias was introduced by the 2012-melt event (Nilsson et al., 2015a). The 20% threshold is less
716 sensitive to these types of changes (Table 1 & 2) and the results are in agreement with previous
717 work that has demonstrated that the 20% threshold best represents the mean surface inside the
718 footprint when exposed to a combination of surface and volume scattering (Davis, 1997).

719 Surface elevation changes, derived from multi-temporal radar altimetry observations, are
720 typically corrected for their correlation to changes in the radar waveform shape. This is to
721 reduce the effect of changes in the volume/surface scattering ratio of the ice sheets surface
722 (Davis, 2005; Flament and Rémy, 2012; Wingham et al., 2006b; Zwally et al., 2005). This
723 inherently adds to the complexity of the processing and analysis, introducing new biases and
724 error sources in the estimated parameters. For the processing approach presented here many

Johan Nilsson 10/4/2016 2:13 PM
Deleted: (

Johan Nilsson 10/4/2016 2:13 PM
Deleted:)

Johan Nilsson 10/9/2016 9:03 PM
Deleted: is

of these steps can be omitted or reduced, as they are an inherent part of the improved waveform retracking. There have been attempts to remove spurious step-changes in elevation resulting from sudden changes in surface scattering characteristics (caused by the 2012 melt event) apparent in the ESA Baseline-B L2 data through post-processing strategies (Nilsson et al., 2015c, and McMillan et al., 2016), but such approaches spread the bias over a longer period of time making the “jumps” less noticeable in the time series by removing the step-change but introduces longer-timescale bias of equal magnitude as the scattering layer is buried by less reflective snow and low-density firn.

Johan Nilsson 10/9/2016 9:16 PM
Deleted:)

Johan Nilsson 10/9/2016 9:16 PM
Deleted: (

The result of the validation procedure shows a larger slope dependent bias in the ESA data, both in the elevation and elevation changes (Figure-1). This is especially true for the surface elevations, which can be seen in the figures of precision and accuracy (Figure 1a and 1c), where both figures show clear linear slope for the ESA surface heights. In comparison, estimated elevations from JPL-product show relatively stable statistics over the entire slope range above 0.2°. The validation of the estimated surface elevation changes, seen in (Figure 1b) and (Figure 1d), shows the effect of the 2012 melt event on the ESA derived elevation changes below 0.2°. Further, the accuracy of the ESA derived changes show a clear negative trend as function of increased surface slope. The derived precision of the surface elevation change increases dramatically above 0.5°, as more complex topography is measured.

The JPL CryoSat-2 processing methodology produces seasonal amplitudes that are in good agreement with those derived from ICESat data, further indicating the processors abilities to track real and physical changes of the ice sheets surface. The current ESA implementation produces noisier estimates of elevation change, as indicated by the larger standard deviations of the residuals in the ESA solutions for the surface-fit and crossover-method. Figure 5 further shows an amplitude bias in the ESA data compared to the corresponding ICESat reference amplitudes. The bias is constant above the Greenland ELA located around 2000 m in altitude but increases linearly as elevations decrease below this. The linear increase in amplitude

seems to be connected to the higher and more variable precipitation in the ablation zone where changes in the variable snow cover produces changes in apparent surface height. This is less prominent for the JPL SIN and LRM retrackers. The estimated seasonal phase in Figure 5c and 5d show that both JPL and ESA CryoSat-2 elevation products can adequately resolve the seasonal maximum of the accumulation signal. Both products provide a timing of the maximum to the month of July over the entire ice sheet, independent of elevation. Assessing the CryoSat-2 derived maximum one does however notice a difference between CryoSat-2 and the reference ICESat dataset. This constitutes roughly a ±1 month difference depending on the elevation and the location. The cause of this difference can be attributed to the temporal sampling of the ICESat mission. During the mission, due to degraded laser lifespan, data was only collected in campaign mode during the spring and winter times corresponding to roughly two months of measurements for each period. When the CryoSat-2 data was resampled to coincide with the ICESat temporal sampling the same elevation and spatial pattern in the phase of the maximum seasonal amplitude was observed as determined from the ICESat data. No corresponding change in amplitude was observed. This was done by selecting CryoSat-2 data corresponding to the same unique months available in the total ICESat record.

The two independent methods used to estimate the volume change of the Greenland Ice Sheet produce consistent volume change estimates. This was especially true for volume changes derived from the JPL elevations, with a discrepancy of less than 1 $km^3 a^{-1}$ between methods. The two methods provided the same estimate of integrated volume change but the use of the surface-fit is recommended as it produces higher spatial sampling compared to the crossover-method and lower errors. The good agreement between the methods further indicates a strong reliability in the estimated volume change rates of the Greenland Ice Sheet over the four-year period. It also shows the ability of CryoSat-2 to capture both small and large-scale spatial patterns in the rugged topography along the coastline and in the interior of

Johan Nilsson 10/4/2016 2:24 PM
Deleted:

Johan Nilsson 10/4/2016 2:24 PM
Deleted: To mimic the temporal sampling of ICESat the each year of the CryoSat-2 data was resampled using the total number of unique months in the ICESat campaign record. This as the specific months used in the ICESat sampling changes with different campaigns.

788 Greenland. This is especially true in the major outlet glacier systems (e.g., Zachariæ Isstrøm,
789 Nioghalvfjerdsfjorden and Storstrømmen).
790 Studying the northern parts of the Greenland Ice Sheet we find that CryoSat-2 captures
791 both intricate and complex behavior in the marginal areas of the ice sheet. This is exemplified in
792 the NE regions of Greenland (Figure 6) near Zacahariæ Isstrøm, Nioghalvfjerdsfjorden and
793 Storstrømmen, which all show complex and localized patterns of elevation change. Here,
794 Nioghalvfjerdsbrae shows very small changes in elevation during the observational time-span,
795 while Zacahariæ Isstrøm, its major neighbor shows large negative trends in elevation change.
796 The observed behavior agrees with the observations made in recent studies by Khan et al.
797 (2014) and Mouginot et al. (2015) who document rapid retreat and drawdown of the ice-front
798 position of the Zacahariæ Isstrøm beginning in 2012. Storstrømmen outlet glacier system also
799 appears to show signs of rapid thinning at low elevations near the ice-front position while a large
800 positive signal is observed roughly 100 km upstream of the terminus. This pattern has also been
801 observed by Joughin et al., (2010) and Thomas et al., (2009), using airborne altimetry and
802 surface velocity mapping. Rates of elevation change from ICESat and CryoSat-2 data show
803 good agreement in basin-scale trends (Figure 6b,c) over the 2003-2009 and 2010-2015 time
804 spans.
805 Mass loss of the Greenland Ice Sheet was estimated for comparison purposes from the Gravity
806 Recovery Climate Experiment (GRACE) satellite for the matching CryoSat-2 time period of
807 2011-2015 (Wiese et al., 2015; Watkins et al., 2015). Converting the estimated mass change to
808 volume change, assuming no changes in firn air content over the study period and an ice
809 density of 917 kg m^{-3} (assessment of changes in firn air content is out of the scope of this
810 paper), gives an ice sheet wide rate of -305 ± 38 km^3 a^{-1} (updated to Schlegel et al., 2016). This
811 estimate is corrected for volume changes from peripheral glaciers that lost volume at a rate of
812 approximately -40 ± 27 km^3 a^{-1} (Box, 2013; Fettweis et al., 2012; Noël et al., 2015). This

Johan Nilsson 10/4/2016 2:26 PM
Deleted: Zacahariae

Johan Nilsson 10/9/2016 9:19 PM
Deleted: two

Johan Nilsson 10/9/2016 9:19 PM
Deleted: systems

Johan Nilsson 10/12/2016 2:56 PM
Deleted: (

817 estimate of peripheral glacier change is in agreement with the estimated volume change of –41
818 ± 8 km^3 a^{-1} from Gardner et al, (2013). The volume rate derived from GRACE data agrees well
819 with our estimated rate from CryoSat-2, where both results are within the 1σ uncertainty of each
820 other and neglecting changes in firn air content over the period of study. The observed volume
821 change rates estimated from this study are within the range of previous studies, ranging from -
822 186 to -309 km^3 a^{-1} for the time period 2003-2009, summarized by Csatho et al. (2014), using
823 the same mass to volume conversion applied to the GRACE data. A more recent study by Helm
824 et al. (2014) of -375 ± 24 km^3 a^{-1} agrees within uncertainties when differences in observation
825 periods (2011 – 2014 vs. 2011 - 2015) are taken into accounted. From this comparison we find
826 that our estimate spans both the estimate of Csatho et al. (2014) and the mass loss estimated
827 from GRACE, while acknowledging the varied time spans of the different studies.

Johan Nilsson 10/12/2016 2:52 PM

Deleted: The observed volume change rates estimated from this study are within the range of previous studies, ranging from -186 to -309 km^3 a^{-1} for the time period 2003-2009, summarized by Csatho et al. (2014). A more recent study by Helm et al. (2014: -375 ± 24 km^3 a^{-1}) agrees within uncertainties when differences in observation periods (2011 – 2014 vs. 2011 - 2015) are taken into accounted. Assuming no changes in firn air content over respective study periods and an ice density of 917 kg m^{-3} we compare estimated changes with corresponding estimates of mass change our estimated rate of Greenland glacier volume change. An assessment of changes in firn air content is out of the scope of this paper. Velicogna et al. (2014) estimated mass loss using the Gravity Recovery and Climate Experiment satellites (GRACE) over the time-period 2003-2013 provided (converted from mass) a rate of -305 ± 63 km^3 a^{-1} for the Greenland which is inclusive of changes in Ice Sheet and peripheral glacier ice mass (–41 ± 8 km^3 a^{-1}, Gardner et al., 2013). The estimated volume change of -265 km^3 a^{-1} from Csatho et al. (2014) and the estimated rate of -305 km^3 a^{-1} from Velicogna et al. (2014) spans our estimated rate of -289 km^3 a^{-1}.

828 9 – Summary and Conclusion

829 We conclude that the use of an adaptive retracker for the SIN-mode, based on the maximum
830 gradient method, and the use of 20% threshold retracker for the LRM-mode provide improved
831 performance to the retracker currently used for the ESA L2 elevation products. It is further
832 important, especially for the SIN-mode, to apply a leading edge discriminator to identify and
833 track the leading edge of the waveform. The functional model currently employed in the ESA
834 processor has, to the author's knowledge, no such discriminator currently implemented. This is
835 important in the SIN-mode, as it often contains multiple surface returns. The single-return model
836 applied in the ESA processor will here have issues fitting a waveform containing multiple
837 surface returns resulting in retrack jitter (Helm et al., 2014).

838 Using the new CryoSat-2 processing methodology for the LRM and SIN-mode we
839 determine the volume change of the Greenland Ice Sheet to be -289 ± 20 km^3 a^{-1} during the
840 period January 2011 to January 2015. The validation against airborne ATM surface elevations
841 and elevation changes showed an average improvement in the RMSE of the measured

elevations of 68% and 27% for the LRM and SIN mode respectively compared to ESA Baseline-B L2 products. The new methodology also provide improved elevation changes with an reduction in RMSE of 55% and 40% for the LRM and SIN mode respectively, compared to their ESA L2 derived counterparts.

The methodology also showed less sensitivity to changes in near-surface scattering properties than equivalent ESA products. The new processing methodology showed little effect of slope-induced errors, providing better performance in the marginal areas of the ice sheets. These improvements to the CryoSat-2 processing mitigate the need for post-processing to correct correlations between changes in surface elevation and changes in the waveform shape (i.e. backscatter and leading edge width etc.) that can introduce biases and add to the complexity of the processing and analysis.

The presented CryoSat-2 processing methodology provides a lower intrinsic error in the measured elevation, elevation change and volume change estimates, all of which will facilitate improved understanding of the geophysical process leading to changes in land ice elevation. Given the release of the ESA Baseline-C, which provides improved corrections and processing mainly for the L1B product, further improvements are expected in the near future.

The complete set of grids used in this study is available for the public from the main author (J. Nilsson) upon request and are provided in geotiff format.

Acknowledgement

We are deeply thankful for the guidance of Laurence Gray and support of David Burgess. We also thank Sebastian Bjerregaard Simonsen for very fruitful discussions. Further, we thank Frank Paul at the University of Zurich for providing us with polygon-outlines of the Greenland Ice Sheet and to the European Space Agency for providing their CryoSat-2 L1b product. We very grateful to the editor E. Berthier, the reviewer L. Schröder and an anonymous reviewer for their

thoughtful and thorough comments that greatly improve the writing and content of the manuscript. We also thank Nicole-Jeanne Schlegel and David Wiese at the Jet Propulsion Laboratory for the use of their GRACE analysis. This publication is contribution 86 of the Nordic Centre of Excellence SVALI funded by the Nordic Top-level Research Initiative. This work was supported by funding from the NASA Cryosphere program. The research was conducted at the Jet Propulsion Laboratory, California Institute of Technology under contract with NASA.

References

Abulaitijiang, A., Andersen, O. B. and Stenseng, L.: Coastal sea level from inland CryoSat-2 interferometric SAR altimetry, Geophys. Res. Lett., 42(6), 1841–1847, doi:10.1002/2015GL063131, 2015.

Arthern, R., Wingham, D. and Ridout, A.: Controls on ERS altimeter measurements over ice sheets: Footprint-scale topography, backscatter fluctuations, and the dependence of microwave penetration depth on satellite orientation, J. Geophys. Res. Atmos., 106(D24), 33471–33484, doi:10.1029/2001JD000498, 2001.

Bales, R. C., Guo, Q., Shen, D., McConnell, J. R., Du, G., Burkhart, J. F., Spikes, V. B., Hanna, E. and Cappelen, J.: Annual accumulation for Greenland updated using ice core data developed during 2000-2006 and analysis of daily coastal meteorological data, J. Geophys. Res. Atmos., 114(6), doi:10.1029/2008JD011208, 2009.

Bamber, J. L.: Ice sheet altimeter processing scheme, Int. J. Remote Sens., 15(4), 925–938, doi:10.1080/01431169408954125, 1994.

Borsa, A. A., Moholdt, G., Fricker, H. A. and Brunt, K. M.: A range correction for ICESat and its potential impact on ice-sheet mass balance studies, Cryosphere, 8(2), 345–357, doi:10.5194/tc-8-345-2014, 2014.

Bouzinac, C.: CryoSat product handbook, European Space Agency, ESA, (https://earth.esa.int/documents/10174/125272/CryoSat_Product_Handbook) (latest checked

October 2016), 2014.

Box, J. E.: Greenland Ice Sheet Mass Balance Reconstruction. Part II: Surface Mass Balance (1840–2010)*, J. Clim., 26(18), 6974–6989, doi:10.1175/JCLI-D-12-00518.1, 2013.

Brenner, A. C., Blndschadler, R. A., Thomas, R. H. and Zwally, H. J.: Slope-induced errors in radar altimetry over continental ice sheets, J. Geophys. Res., 88(C3), 1617, doi:10.1029/JC088iC03p01617, 1983.

Brenner, A. C. ., DiMarzio, J. P. . and Zwally, H. J. .: Precision and accuracy of satellite radar and laser altimeter data over the continental ice sheets, IEEE Trans. Geosci. Remote Sens., 45(2), 321–331, doi:10.1109/TGRS.2006.887172, 2007.

Csatho, B. M., Schenk, A. F., van der Veen, C. J., Babonis, G., Duncan, K., Rezvanbehbahani, S., van den Broeke, M. R., Simonsen, S. B., Nagarajan, S. and van Angelen, J. H.: Laser altimetry reveals complex pattern of Greenland Ice Sheet dynamics., Proc. Natl. Acad. Sci. U. S. A., 111(52), 18478–83, doi:10.1073/pnas.1411680112, 2014.

Davis, C. H.: Surface and volume scattering retracking algorithm for ice sheet satellite altimetry, IEEE Trans. Geosci. Remote Sens., 31(4), 811–818, doi:10.1109/36.239903, 1993.

Davis, C. H.: A robust threshold retracking algorithm for measuring ice-sheet surface elevation change from satellite radar altimeters, IEEE Trans. Geosci. Remote Sens., 35(4), 974–979, doi:10.1109/36.602540, 1997.

Davis, C. H.: Snowfall-Driven Growth in East Antarctic Ice Sheet Mitigates Recent Sea-Level Rise, Science (80-.)., 308(5730), 1898–1901, doi:10.1126/science.1110662, 2005.

Davis, C. H. and Ferguson, A. C.: Elevation change of the antarctic ice sheet, 1995-2000, from ERS-2 satellite radar altimetry, IEEE Trans. Geosci. Remote Sens., 42(11), 2437–2445, doi:10.1109/TGRS.2004.836789, 2004.

Ettema, J., Van Den Broeke, M. R., Van Meijgaard, E., Van De Berg, W. J., Bamber, J. L., Box, J. E. and Bales, R. C.: Higher surface mass balance of the Greenland ice sheet revealed by high-resolution climate modeling, Geophys. Res. Lett., 36(12), 1–5,

944 doi:10.1029/2009GL038110, 2009.
945 Fettweis, X., Franco, B., Tedesco, M., van Angelen, J. H., Lenaerts, J. T. M., van den Broeke,
946 M. R. and Gallée, H.: Estimating Greenland ice sheet surface mass balance contribution to
947 future sea level rise using the regional atmospheric climate model MAR, Cryosph., 7, 469–489,
948 doi:10.5194/tcd-6-3101-2012, 2012.
949 Flament, T. and Rémy, F.: Dynamic thinning of Antarctic glaciers from along-track repeat radar
950 altimetry, J. Glaciol., 58(211), 830–840, doi:10.3189/2012JoG11J118, 2012.
951 Galin, N., Wingham, D. J., Cullen, R., Fornari, M., Smith, W. H. F. and Abdalla, S.: Calibration of
952 the CryoSat-2 interferometer and measurement of across-track ocean slope, IEEE Trans.
953 Geosci. Remote Sens., 51(1), 57–72, doi:10.1109/TGRS.2012.2200298, 2013.
954 Gardner, A. S., Moholdt, G., Cogley, J. G., Wouters, B., Arendt, A. a, Wahr, J., Berthier, E.,
955 Hock, R., Pfeffer, W. T., Kaser, G., Ligtenberg, S. R. M., Bolch, T., Sharp, M. J., Hagen, J. O.,
956 van den Broeke, M. R. and Paul, F.: A reconciled estimate of glacier contributions to sea level
957 rise: 2003 to 2009., Science, 340(6134), 852–7, doi:10.1126/science.1234532, 2013.
958 Gray, L., Burgess, D., Copland, L., Cullen, R., Galin, N., Hawley, R. and Helm, V.:
959 Interferometric swath processing of Cryosat data for glacial ice topography, Cryosph., 7(6),
960 1857–1867, doi:10.5194/tc-7-1857-2013, 2013.
961 Gray, L., Burgess, D., Copland, L., Demuth, M. N., Dunse, T., Langley, K. and Schuler, T. V.:
962 CryoSat-2 delivers monthly and inter-annual surface elevation change for Arctic ice caps,
963 Cryosph., 9(5), 1895–1913, doi:10.5194/tc-9-1895-2015, 2015.
964 Helm, V., Humbert, A. and Miller, H.: Elevation and elevation change of Greenland and
965 Antarctica derived from CryoSat-2, Cryosph., 8(4), 1539–1559, doi:10.5194/tc-8-1539-2014,
966 2014.
967 Herzfeld, U. C.: Least-squares collocation, geophysical inverse theory and geostatistics: a bird's
968 eye view, Geophys. J. Int., 111(2), 237–249, doi:10.1111/j.1365-246X.1992.tb00573.x, 1992.
969 Howat, I. M., Smith, B. E., Joughin, I. and Scambos, T. A.: Rates of southeast Greenland ice

970 volume loss from combined ICESat and ASTER observations, Geophys. Res. Lett., 35(17), 1–5,
971 doi:10.1029/2008GL034496, 2008.
972 Howat, I. M., Negrete, A. and Smith, B. E.: The Greenland Ice Mapping Project (GIMP) land
973 classification and surface elevation data sets, Cryosph., 8(4), 1509–1518, doi:10.5194/tc-8-
974 1509-2014, 2014.
975 Joughin, I., Smith, B. E., Howat, I. M., Scambos, T. and Moon, T.: Greenland flow variability
976 from ice-sheet-wide velocity mapping, J. Glaciol., 56(197), 415–430,
977 doi:10.3189/002214310792447734, 2010.
978 Keith Raney, R.: The delay/doppler radar altimeter, IEEE Trans. Geosci. Remote Sens., 36(5),
979 1578–1588, doi:10.1109/36.718861, 1998.
980 Khan, S. a, Kjaer, K. H., Bevis, M., Bamber, J. L., Wahr, J., Kjeldsen, K. K., Bjork, A. a,
981 Korsgaard, N. J., Stearns, L. a, van den Broeke, M. R., Liu, L., Larsen, N. K. and Muresan, I. S.:
982 Sustained mass loss of the northeast Greenland ice sheet triggered by regional warming, Nat.
983 Clim. Chang., 4(4), 292–299, doi:10.1038/nclimate2161, 2014.
984 Khvorostovsky, K. S.: Merging and Analysis of Elevation Time Series Over Greenland Ice Sheet
985 From Satellite Radar Altimetry, IEEE Trans. Geosci. Remote Sens., 50(1), 23–36,
986 doi:10.1109/TGRS.2011.2160071, 2012.
987 Krabill, W. B., Abdalati, W., Frederick, E. B., Manizade, S. S., Martin, C. F., Sonntag, J. G.,
988 Swift, R. N., Thomas, R. H. and Yungel, J. G.: Airborne laser altimetry mapping of the
989 Greenland ice sheet : application to mass balance assessment, J. Geodyn., 34, 357–376,
990 doi:10.1016/s0264-3707(02)00048-0, 2002.
991 Lacroix, P., Dechambre, M., Legrésy, B., Blarel, F. and Rémy, F.: On the use of the dual-
992 frequency ENVISAT altimeter to determine snowpack properties of the Antarctic ice sheet,
993 Remote Sens. Environ., 112, 1712–1729, doi:10.1016/j.rse.2007.08.022, 2008.
994 Lewis, S. M. and Smith, L. C.: Hydrologic drainage of the Greenland Ice Sheet, Hydrol.
995 Process., 23(14), 2004–2011, doi:10.1002/hyp.7343, 2009.

McMillan, M., Leeson, A., Shepherd, A., Briggs, K., Armitage, T. W. K., Hogg, A., Kuipers Munneke, P., van den Broeke, M., Noël, B., van de Berg, W. J., Ligtenberg, S., Horwath, M., Groh, A., Muir, A. and Gilbert, L.: A high-resolution record of Greenland mass balance, Geophys. Res. Lett., 43(13), 7002–7010, doi:10.1002/2016GL069666, 2016.

Moholdt, G., Nuth, C., Hagen, J. O. and Kohler, J.: Recent elevation changes of Svalbard glaciers derived from ICESat laser altimetry, Remote Sens. Environ., 114(11), 2756–2767, doi:10.1016/j.rse.2010.06.008, 2010.

Mouginot, J., Rignot, E., Scheuchl, B., Fenty, I., Khazendar, A., Morlighem, M., Buzzi, A. and Paden, J.: Fast retreat of Zachariae Isstrom, northeast Greenland, Science (80-.)., 350(6266), 1357–1361, doi:10.1126/science.aac7111, 2015.

Nilsson, J., Vallelonga, P., Simonsen, S. B., Sørensen, L. S., Forsberg, R., Dahl-Jensen, D., Hirabayashi, M., Goto-Azuma, K., Hvidberg, C. S., Kjaer, H. A. and Satow, K.: Greenland 2012 melt event effects on CryoSat-2 radar altimetry, Geophys. Res. Lett., 42(10), 3919–3926, doi:10.1002/2015GL063296, 2015a.

Nilsson, J., Sandberg Sørensen, L., Barletta, V. R. and Forsberg, R.: Mass changes in Arctic ice caps and glaciers: implications of regionalizing elevation changes, Cryosph., 9(1), 139–150, doi:10.5194/tc-9-139-2015, 2015b.

Nilsson, J, Forsberg, R and Sandberg Sørensen, L.: Cryosphere Monitoring from Satellites and Aircrafts, Ph.D. thesis, Technical University of Denmark, Kgs. Lyngby, 2015c.

Noël, B., van de Berg, W. J., van Meijgaard, E., Kuipers Munneke, P., van de Wal, R. S. W. and van den Broeke, M. R.: Evaluation of the updated regional climate model RACMO2.3: summer snowfall impact on the Greenland Ice Sheet, Cryosph., 9(5), 1831–1844, doi:10.5194/tc-9-1831-2015, 2015.

Poinar, K., Joughin, I., Das, S. B., Behn, M. D., Lenaerts, J. T. M. and van den Broeke, M. R.: Limits to future expansion of surface-melt-enhanced ice flow into the interior of western Greenland, Geophys. Res. Lett., 42(6), 1800–1807, doi:10.1002/2015GL063192, 2015.

1022 Remy, F., Mazzega, P., Houry, S., Brossier, C. and Minster, J. F.: Mapping of the topography of
1023 continental ice by inversion of satellite-altimeter data, J. Glaciol., 35(119), 98–107,
1024 doi:10.3189/002214389793701419, 1989.
1025 Remy, F., Flament, T., Blarel, F. and Benveniste, J.: Radar altimetry measurements over
1026 antarctic ice sheet: A focus on antenna polarization and change in backscatter problems, Adv.
1027 Sp. Res., 50(8), 998–1006, doi:10.1016/j.asr.2012.04.003, 2012.
1028 Sasgen, I., van den Broeke, M., Bamber, J. L., Rignot, E., Sørensen, L. S., Wouters, B.,
1029 Martinec, Z., Velicogna, I. and Simonsen, S. B.: Timing and origin of recent regional ice-mass
1030 loss in Greenland, Earth Planet. Sci. Lett., 333–334, 293–303, doi:10.1016/j.epsl.2012.03.033,
1031 2012.
1032 Shepherd, A., Ivins, E. R., A, G., Barletta, V. R., Bentley, M. J., Bettadpur, S., Briggs, K. H.,
1033 Bromwich, D. H., Forsberg, R., Galin, N., Horwath, M., Jacobs, S., Joughin, I., King, M. A.,
1034 Lenaerts, J. T. M., Li, J., Ligtenberg, S. R. M., Luckman, A., Luthcke, S. B., McMillan, M.,
1035 Meister, R., Milne, G., Mouginot, J., Muir, A., Nicolas, J. P., Paden, J., Payne, A. J., Pritchard,
1036 H., Rignot, E., Rott, H., Sorensen, L. S., Scambos, T. A., Scheuchl, B., Schrama, E. J. O.,
1037 Smith, B., Sundal, A. V., van Angelen, J. H., van de Berg, W. J., van den Broeke, M. R.,
1038 Vaughan, D. G., Velicogna, I., Wahr, J., Whitehouse, P. L., Wingham, D. J., Yi, D., Young, D.
1039 and Zwally, H. J.: A Reconciled Estimate of Ice-Sheet Mass Balance, Science (80-.).,
1040 338(6111), 1183–1189, doi:10.1126/science.1228102, 2012.
1041 Sørensen, L. S., Simonsen, S. B., Nielsen, K., Lucas-Picher, P., Spada, G., Adalgeirsdottir, G.,
1042 Forsberg, R. and Hvidberg, C. S.: Mass balance of the Greenland ice sheet (2003-2008) from
1043 ICESat data - The impact of interpolation, sampling and firn density, Cryosphere, 5(1), 173–186,
1044 doi:10.5194/tc-5-173-2011, 2011.
1045 Sørensen, L. S., Simonsen, S. B., Meister, R., Forsberg, R., Levinsen, J. F. and Flament, T.:
1046 Envisat-derived elevation changes of the Greenland ice sheet, and a comparison with ICESat
1047 results in the accumulation area, Remote Sens. Environ., 160, 56–62,

1048 doi:10.1016/j.rse.2014.12.022, 2015.
1049 Thomas, R., Frederick, E., Krabill, W., Manizade, S. and Martin, C.: Recent changes on
1050 Greenland outlet glaciers, J. Glaciol., 55(189), 147–162, doi:10.3189/002214309788608958,
1051 2009.
1052 Watkins, M. M., Wiese, D. N., Yuan, D., Boening, C. and Landerer, F. W.: Improved methods for
1053 observing Earth's time variable mass distribution with GRACE using spherical cap mascons, J.
1054 Geophys. Res. Solid Earth, 120(4), 2648–2671, doi:10.1002/2014JB011547, 2015.
1055 Wenlu Qi and Braun, A.: Accelerated elevation change of Greenland's Jakobshavn glacier
1056 observed by ICESat and IceBridge, IEEE Geosci. Remote Sens. Lett., 10(5), 1133–1137,
1057 doi:10.1109/LGRS.2012.2231954, 2013.
1058 Wiese, D. N., Yuan, D.-N., Boening, C., Landerer, F. W., and Watkins, M. M.: JPL GRACE
1059 Mascon Ocean, Ice, and Hydrology Equivalent Water Height RL05M.1 CRI Filtered, Ver. 2,
1060 PO.DAAC, CA, USA, doi:10.5067/TEMSC-OLCR5, 2015.
1061 Wingham, D. J., Rapley, C. G. and Griffiths, H.: New Techniques in Satellite Altimeter Tracking
1062 Systems, in Proceedings of the IGARSS Symposium, Zurich, pp. 1339–1344, ESA SP-254,
1063 Zurich., 1986.
1064 Wingham, D. J., Francis, C. R., Baker, S., Bouzinac, C., Brockley, D., Cullen, R., de Chateau-
1065 Thierry, P., Laxon, S. W., Mallow, U., Mavrocordatos, C., Phalippou, L., Ratier, G., Rey, L.,
1066 Rostan, F., Viau, P. and Wallis, D. W.: CryoSat: A mission to determine the fluctuations in
1067 Earth's land and marine ice fields, Adv. Sp. Res., 37(4), 841–871,
1068 doi:10.1016/j.asr.2005.07.027, 2006a.
1069 Wingham, D. J., Shepherd, a, Muir, a and Marshall, G. J.: Mass balance of the Antarctic ice
1070 sheet., Philos. Trans. A. Math. Phys. Eng. Sci., 364(1844), 1627–35,
1071 doi:10.1098/rsta.2006.1792, 2006b.
1072 Wouters, B., Martin-Espanol, A., Helm, V., Flament, T., van Wessem, J. M., Ligtenberg, S. R.
1073 M., van den Broeke, M. R. and Bamber, J. L.: Dynamic thinning of glaciers on the Southern

1074 Antarctic Peninsula, Science (80-.)., 348(6237), 899–903, doi:10.1126/science.aaa5727, 2015.
1075 Zwally, H. J., Bindschadler, R. a, Brenner, a C., Major, J. a and Marsh, J. G.: Growth of
1076 greenland ice sheet: measurement., Science, 246(4937), 1587–1589,
1077 doi:10.1126/science.246.4937.1587, 1989.
1078 Zwally, H. J., Giovinetto, M. B., Li, J., Cornejo, H. G. and Beckley, M. a: Mass changes of the
1079 Greenland and Antarctica ice sheets and shelves and contributions to sea level rise: 1992-2002,
1080 J. Glaciol., 51(175), 509, doi:10.3189/172756505781829007, 2005.
1081 Zwally, H. J., Jun, L., Brenner, A. C., Beckley, M., Cornejo, H. G., Dimarzio, J., Giovinetto, M.
1082 B., Neumann, T. a, Robbins, J., Saba, J. L., Donghui, Y. and Wang, W.: Greenland ice sheet
1083 mass balance: distribution of increased mass loss with climate warming; 2003–07 versus 1992–
1084 2002, J. Glaciol., 57(201), 88–102, doi:10.3189/002214311795306682, 2011.
1085 Zwally, H. Jay, Mario B. Giovinetto, Matthew A. Beckley, and Jack L. Saba: Antarctic and
1086 Greenland drainage systems, GSFC Cryospheric Sciences Laboratory, at
1087 http://icesat4.gsfc.nasa.gov/cryo_data/ant_grn_drainage_systems.php, 2012

Tables:

Table 1: Accuracy (Mean), precision (SD) and the total RMS-error (RMSE) of surface elevation from CryoSat-2 observations compared to IceBridge ATM elevations. Here, the LRM mode represents the interior of the ice sheet and SIN the marginal high relief areas.

JPL	**Mean (m)**	**SD (m)**	**RMSE (m)**
LRM	0.00	0.43	0.45
SIN	-0.52	0.58	0.82
ESA	**Mean (m)**	**SD (m)**	**RMSE (m)**
LRM	-1.06	0.89	1.40
SIN	-0.90	1.05	1.13

Table 2: Accuracy (Mean), precision (SD) and the total RMS-error (RMSE) of surface elevation changes from CryoSat-2 derived from two independent methods [Surface Fit (SF) and the Crossover (XO) method], compared to IceBridge ATM data.

JPL - LRM	**Mean (m)**	**SD (m)**	**RMSE (m)**
SF	0.11	0.67	0.70
XO	0.24	0.72	0.78
ESA - LRM	**Mean (m)**	**SD (m)**	**RMSE (m)**
SF	0.25	1.51	1.57
XO	0.60	1.02	1.20
JPL - SIN	**Mean (m)**	**SD (m)**	**RMSE (m)**
SF	0.30	0.58	0.66
XO	-0.60	1.26	1.26
ESA - SIN	**Mean (m)**	**SD (m)**	**RMSE (m)**
SF	0.34	1.06	1.11
XO	-0.21	1.44	1.44

Table 3: Validation of four different DEMs, compared to IceBridge ATM elevation data. Based on the weighted (number of samples) average of the four different ATM campaigns from 2011 to 2014. Elevation values at each ATM location were estimated by bilinear interpolation for each DEM product.

DEM	Mean (m)	SD (m)	RMSE (m)
AWI	-1.35	5.95	6.12
GIMP	-1.13	7.22	7.32
JPL	-0.87	6.31	6.39
ESA	-2.83	6.13	6.76

Table 4: Individual basin volume changes (km^3a^{-1}) for the Surface-Fit (SF) and Crossover (XO) method for the JPL and ESA product for the time period Jan-2011 to Jan-2015, with corresponding volumetric error.

Basin	SF – JPL	XO – JPL	SF - ESA	XO - ESA
1	-26 ± 8	-23 ± 12	-9 ± 14	-11 ± 15
2	5 ± 8	0 ± 13	31 ± 16	30 ±16
3	-38 ± 9	-34 ± 19	-46 ± 16	-31 ± 23
4	-36 ± 7	-37 ± 15	-42 ± 12	-16 ± 18
5	-19 ± 4	-27 ± 11	-19 ± 7	-6 ± 13
6	-72 ± 7	-71 ± 12	-75 ± 13	-79 ± 18
7	-56 ± 7	-51 ± 10	-41 ± 14	-35 ± 15
8	-48 ± 8	-45 ± 12	-23 ± 15	-27 ± 17
TOT	**-289 ± 20**	**-288 ± 37**	**-224± 38**	**-174 ± 48**

Figures:

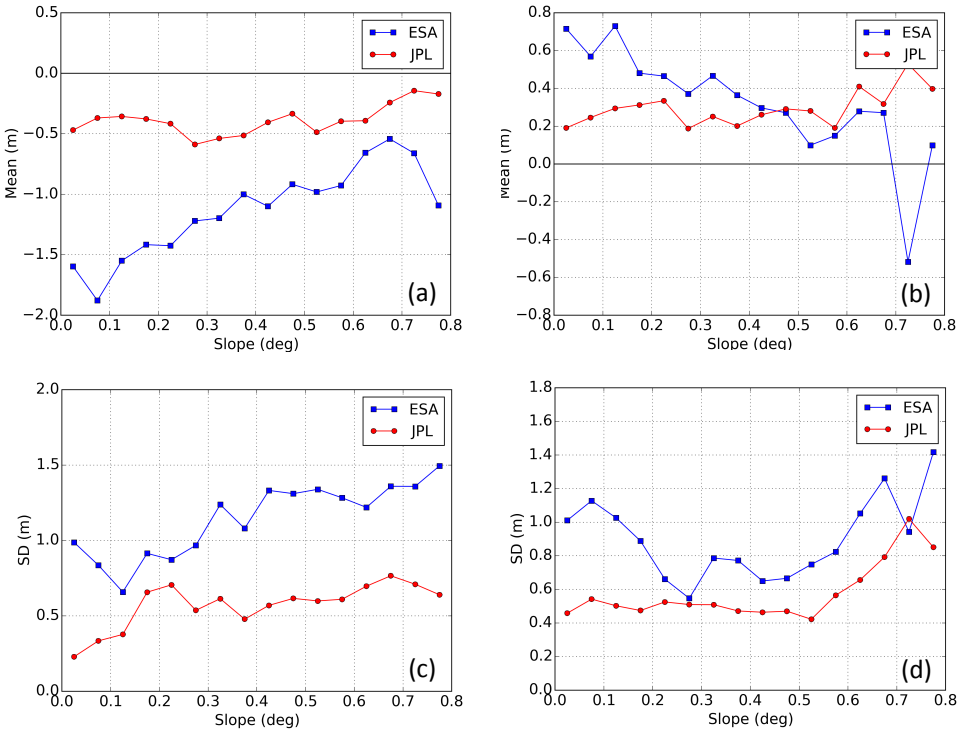

Figure 1: Validation of surface elevations (2012) (a,c) and surface elevation changes (2011-2014) (b,d) compared to IceBridge ATM, as a function of surface slope. The accuracy of the measurement is defined as the mean-value (Mean) of the CryoSat-2-ATM residuals and the precision as the standard deviation (SD).

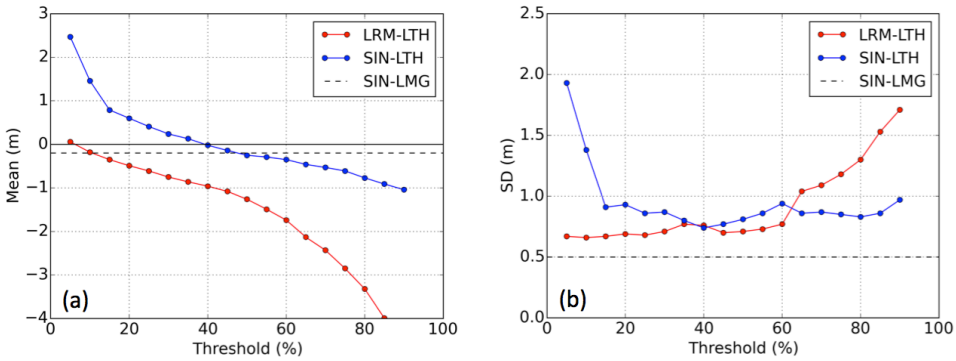

Figure 2: Comparison of accuracy (a) and precision (b) as a function retracking threshold for the leading edge threshold retracker (LTH, dots) applied to the of the LRM (red) and SIN (blue) data and the leading edge maximum gradient retracker (LMG, dashed grey line) applied to the SIN data over Jakobshavn Isbræ and the region around the NEEM camp (77°27'N 51°3.6'W). The accuracy (mean) and the precision (standard deviation) has for each threshold level been determined using near coincident ATM elevation within a search radius of 50 m. The statistics was estimated using CryoSat-2 data from March-May 2013 and compared to ATM data from April 2013.

Johan Nilsson 10/5/2016 11:49 AM
Formatted: Font:(Default) Arial, Italic

Johan Nilsson 10/5/2016 11:49 AM
Formatted: Centered

Johan Nilsson 10/5/2016 11:49 AM
Formatted: Font:(Default) Arial, Italic

Johan Nilsson 10/5/2016 11:49 AM
Formatted: Font:(Default) Arial, Italic

Johan Nilsson 10/5/2016 11:49 AM
Formatted: Font:(Default) Arial, Italic

Johan Nilsson 10/5/2016 11:49 AM
Formatted: Font:(Default) Arial, Italic

Johan Nilsson 10/5/2016 11:49 AM
Formatted: Font:(Default) Arial, Italic

Johan Nilsson 10/5/2016 11:49 AM
Formatted: Font:(Default) Arial, Italic

Johan Nilsson 10/5/2016 11:49 AM
Formatted: Font:Italic

Johan Nilsson 10/5/2016 11:48 AM
Deleted: :

Johan Nilsson 10/4/2016 2:33 PM
Deleted:

Johan Nilsson 10/5/2016 11:48 AM
Deleted: *Accuracy (a) and precision (b) of JPL surface elevations, relative to near-coincident ATM elevations, estimated from a Leading-edge Threshold retracker (LTH, dots) over Jakobshavn and NE-Greenland and the Leading-edge Maximum Gradient (LMG retracker, (dashed grey line) for the SIN-mode. The accuracy is defined as the mean-value (Mean) of the CryoSat-2-ATM residuals and the precision as the standard deviation (SD).*

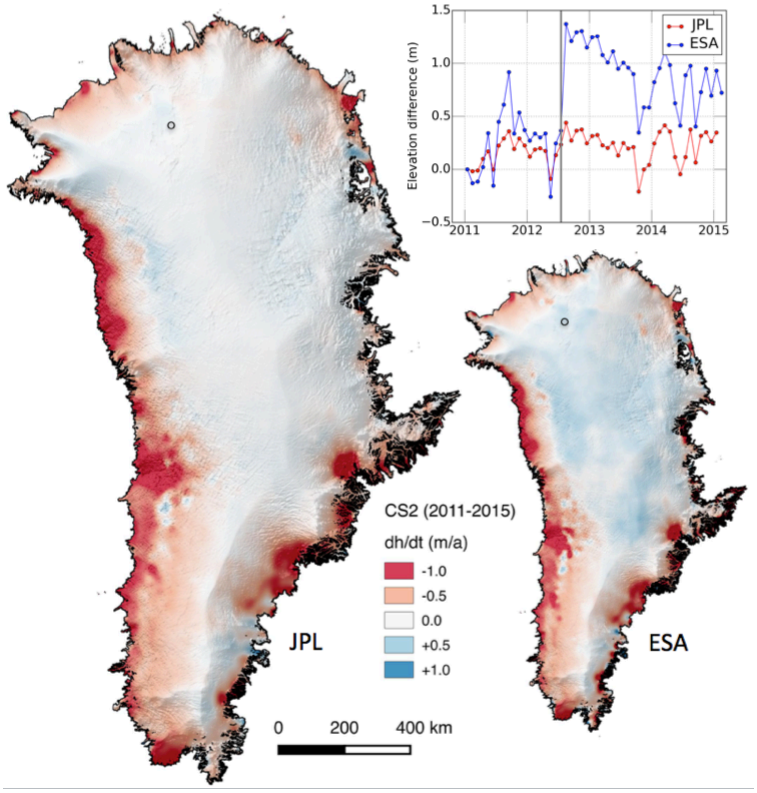

Figure 3: 2011-2015 elevation changes estimated from the surface-fit methods for the estimated L2 products. The time series depicted in the figure has been extracted at the NEEM camp (77°27'N 51°3.6'W), indicated by the black circle in both maps. The time series show the effect of the 2012 melt event, indicated by the grey vertical line, on the retrieved surface elevations. The JPL product produced a total volume change of -289 ± 20 $km^3 a^{-1}$ while the estimated total volume change of the ESA product was -224 ± 38 $km^3 a^{-1}$. This corresponds to -29 versus 38 $km^3 a^{-1}$ (H > 2000 m) and -259 versus -262 $km^3 a^{-1}$ (H < 2000 m) for the JPL and ESA product respectively. Images have been smoothed with a 10 km median filter for visualization purposes. The 1x1 km ice sheets mask used in this figure was constructed from polygons obtained from Frank Paul at the University of Zurich (personal communication).

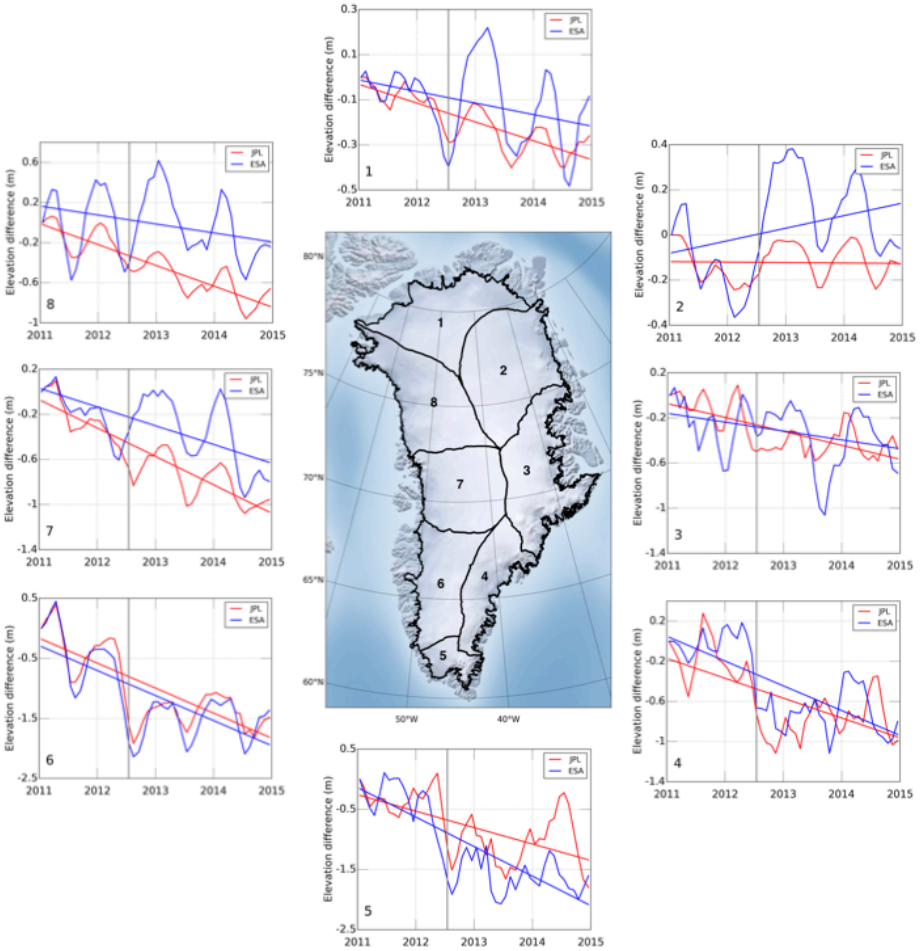

Figure 4. Monthly elevation change time-series for 8 large drainage basins of the Greenland Ice Sheet. Time-series have been smoothed using a 3-month moving average for improved visualization. The grey vertical line indicates the timing of the 2012 melt event.

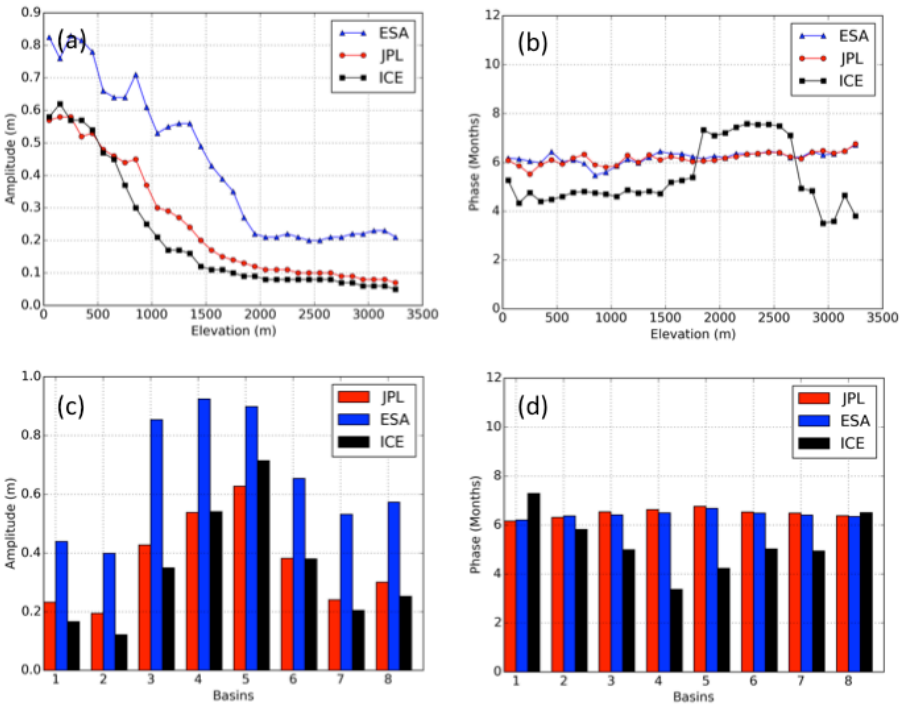

Figure 5: Estimated seasonal amplitude (a,c) and phase of the maximum amplitude (b,d) from the surface-fit method for CryoSat-2 [ESA (blue) and JPL (red)] compared to ICESat (ICE, black)). Values are compared using a search radius of 50 m, using the closest point within this distance, and the phase offset is referenced from 1st of January. The values of amplitude and phase are then binned according to elevation using the median value within 100 m intervals.

Johan Nilsson 10/16/2016 5:00 PM
Deleted: .

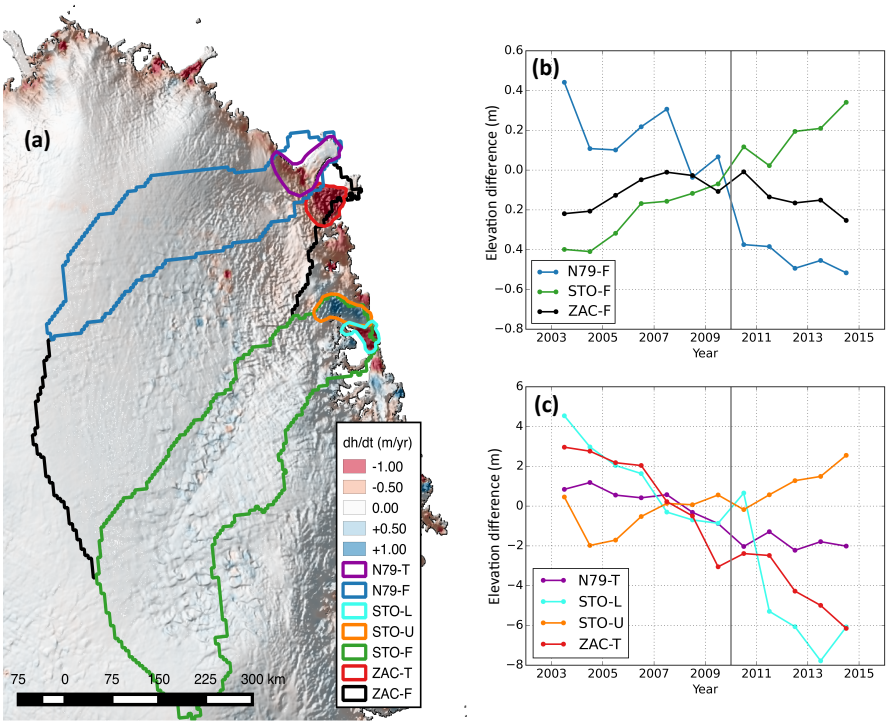

Figure 6: Northeast part of the Greenland Ice Sheet showing surface elevation change (a) from CryoSat-2 JPL-solution (2011-2015), with corresponding hydrological basin outlines. The hydrological basins are separated into full basins size (b) and to the terminus areas (c). Sub-figures (b) and (c) shows a merged 12 year annual elevation time series from ICESat and CryoSat-2 for each color-coded area in (a). The derived elevation time series was formed using the surface-fit method described in Section (3.1) onto a 500 m grid to facilitate merging of the two data sets due to their difference in orbit characteristics. The elevation change map is overlaid onto the CryoSat-2 hill shaded DEM based on surface heights from Jul-2010 to Feb-2015. The annual 12-year time series was created from the surface-fit method by binning the monthly values into annual values using the median of the corresponding 12 months.

Rebuttal to editor for tc-2016-109

We would like to thank the editor for his thoughtful and thorough review our manuscript, which has been a great help for improving the manuscript. We have tried to accommodate all of the editor's suggestions. We summarized our response to each comment below and included a tracked document with the corresponding changes. During the process of applying the editors correct we further added small changes to the document relating to grammar and text structure, which are visible in the tracked changes.

The editor's comments are marked using (E) and the corresponding response below with (R).

Main manuscript:

(E) L10-14 Split into two sentences? It seems the wording could be improved here. Quite important for the first sentences of the abstract

(R) We split the sentence into two different sentences and further added some text to tie them together.

(E) L154 "Larger than... unknown". Check that wording is OK.

(R) Wording checked and changed accordingly.

(E) L186 delete "," after Davis

(R) "," has been deleted

(E) L191 retracking

(R) Has been corrected accordingly

(E) 468. This is wrong. The glacier mask is based on data from this time period. But the altimetry data (ICESat, ASTER, SPIRIT) are not from this period. Check carefully.

(R) We thank the editor for pointing this out and we have changed and updated the sentence to read "from the mid 1990's to 2010 (depending on data source)".

(E) 515 "that" repeated

(R) Changed accordingly

(E) L528. "that" repeated

(R) Changed accordingly

(E) L543 effect?

(R) Changed to read “effect”

(E) L551. "by" instead of "with"?

(R) Changed to “by”

(E) L553. This is especially

(R) Changed accordingly

(E) L565. Homogeneity of the equation. Authors need I think to divide the right term by (Alrm+Asin)

(R) The error in (13) represent the volume change error in (km^3a^{-1}), so we can not divide by (A_{tot}). But, we have changed the paragraph to make it more clear when we are referring to volume or elevation change, as it was a bit confusing in the manuscript.

(E) What about organizing the Results in some subsections? Accuracy/precision against ATM and then 2011-2015 dh/dt. Would help the different types of readers to find the relevant information.

(R) We have divided the results into three sections based on elevation, elevation change and volume change. Hopefully, this will help to improve the readability of the section to obtain a better overview.

(E) L655 "an" rather than "a"

(R) Changed accordingly

(E) L685. Add "a" or "b" to this reference

(R) References has been updated

(E) L708. "Can mostly related to". "be" missing?

(R) Correct and has been changed accordingly

(E) L718. Do the authors have a reference for the 2000 m altitude for the ELA of the GIS?

(R) We added the following reference to the manuscript: “Limits to future expansion of surface-melt-enhanced ice flow into the interior of western Greenland” doi: 10.1002/2015GL063192

(E) L771. Where does the sentence end/start?

(R) We corrected the sentence by adding punctuation between “purposes” and “These”.

(E) L777. Sorry it is unclear to me what are these two time periods. Could the authors clarify?

(R) We have added the two time periods in the sentence (2003-2009 and 2010-2015).

(E) L818. Delete parenthesis

(R) Changed accordingly

(E) L883-L886. Check wording and improve if you think it is necessary. Also I miss here a clear description of the results obtained when "mimicing" the ICESat temporal sampling in the CS2 data. You did it right?

(R) Yes, we used the same months (total unique number) for CryoSat-2 as used in the ICESat data. The sentence was difficult so understand so we have rewritten to hopefully make it clearer.

(E) L912. Correct spelling for " Zacahariæ"

(R) Changed accordingly

(E) L930. Clarify that this is your value for 2011-2015 (right?). Given the large difference between your estimates for 2011-2014 and 2011-2015, is it worth comparing your estimate to GRACE data for 2003-2014, i.e. a really different time period? The agreement could be entirely coincidental...Can you get GRACE data for 2011-2015 (or 2011-2014 from Velicogna?) and compare apple and apple i.e. exact same time period? That would be much more convincing...

(R) This section has now been rewritten and we have instead of Velicogna used estimates from the JPL Mascon solution, see [1], to estimate a mass loss trend for the period 2011-2015, which shows good agreement with out own estimate from CryoSat-2, acknowledging the simple assumption made to convert from mass to volume, using a density of 917 kg/m^3.

(E) L1161. "and' here

(R) Changed accordingly

(E) Figure 2. Authors need to describe in a few words what is the "threshold" shown in the X-axis. To make the figure self-consistent. Right now hard to approach without carefully re-reading the corresponding text.

(R) We have rewritten the entire caption to make it more standalone which we hope will improve the readability and understanding of the figure.

(E) We do not see much from the color scale. Limit transparency?

(R) We played around with the transparency when producing the figure and we feel that the current format provided the best tradeoff between detail and transparency. Hopefully, the editor will find this acceptable.

Supplement:

(E) L82. “individual” -> “separately” (I think)

(R) Changed accordingly

References:

[1] Wiese, D. N., Yuan, D.-N., Boening, C., Landerer, F. W., and Watkins, M. M.: JPL GRACE Mascon Ocean, Ice, and Hydrology Equivalent Water Height RL05M.1 CRI Filtered, Ver. 2, PO.DAAC, CA, USA, doi:10.5067/TEMSC-OLCR5, 2015.